

In Situ Determination of Speciation and Local Structure of NaCl–SrCl₂ and LiF–ZrF₄ Molten Salts

Timothy J. Lynch,[†] Nancy R. Birkner,[†] Matthew S. Christian, Jacob A. Wrubel, Juliano Schorne-Pinto, Arjen Van Veelen, John R. Bargar, Theodore M. Besmann, Kyle S. Brinkman, and Wilson K. S. Chiu*



Cite This: <https://doi.org/10.1021/acs.jpcb.1c07552>



Read Online

ACCESS |



Metrics & More

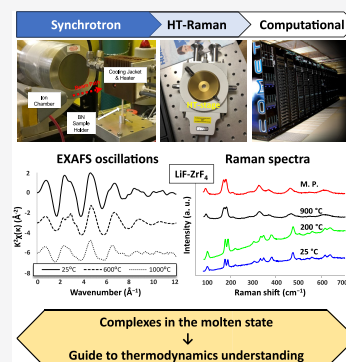


Article Recommendations



Supporting Information

ABSTRACT: Understanding the local environment of the metal atoms in salt melts is important for modeling the properties of melts and predicting their behavior and thus helping enable the development of technologies such as molten salt reactors and solar-thermal power systems and new approaches to recycling rare-earth metals. Toward that end, we have developed an *in situ* approach for measuring the coordination of metals in molten salt coupling X-ray absorption spectroscopy (XAS) and Raman spectroscopy. Our approach was demonstrated for two salt mixtures (1.9 and 5 mol % SrCl₂ in NaCl, 0.8 and 5 mol % ZrF₄ in LiF) at up to 1100 °C. Near-edge (X-ray absorption near-edge structure, XANES) and extended X-ray absorption fine structure (EXAFS) spectra were measured. The EXAFS response was modeled using *ab initio* FEFF calculations. Strontium's first shell is observed to be coordinated with chlorine (Sr²⁺–Cl[–]) and zirconium's first shell is coordinated by fluorine (Zr⁴⁺–F[–]), both having coordination numbers that decrease with increasing temperature. Multiple zirconium complexes are believed to be present in the melt, which may interfere and distort the EXAFS spectra and result in an anomalously low zirconium first shell coordination number. The use of boron nitride (BN) powder as a salt diluent for XAFS measurements was found to not interfere with measurements and thus can be used for investigations of such systems.



1. INTRODUCTION

The local structure and dynamics of molten salts is important for understanding and modeling their properties and predicting their behavior. This is helpful in enabling the development of technologies such as molten salt reactors, nuclear fuel processing, solar-thermal power systems and new approaches to recycling rare-earth metals. The local structure reflects solution properties such as composition/speciation, oxidation state, precipitating solid phases (melting points), phase formation, chemical potentials/redox for controlling corrosion and transport, viscosity, and vapor pressures.

The structure and dynamics of molten salts have been investigated over the past five decades using NMR spectroscopy,¹ Raman spectroscopy,² ultraviolet–visible–infrared (UV–vis–IR) spectroscopy,³ and X-ray absorption spectroscopy (XAS)^{4–6} to determine physical and chemical properties.^{7–10} The spectroscopic and scattering methods have the specificity and sensitivity to measure the change of the actinide oxidation state, e.g., the reduction of U(IV) to U(III) in high-temperature alkali chloride melts,³ as well as the local structure and bonding of species in solution such as interatomic distances and coordination numbers.^{11,12} Additionally, computer-based simulations have previously been shown to be robust in predicting thermal properties.^{8,9,13,14} Combining instrumental and computational approaches allows the study of molten salts to high temperature to determine how local structure impacts physical and chemical properties.

Despite the capabilities noted above, the study of a molten salt's local structure has received limited attention due to the challenging environment and the complex interaction of the ions, and therefore, novel approaches are required for analyzing local coordination. Among these, one is Raman spectroscopy, which measures vibrational modes that correlate with specific molecular orbital geometries. Structural, compositional, and thermal changes influence active Raman vibrational modes² making it an appropriate tool for elucidating behavior. For instance, an increase in atomic interactions, such as a shortened bond distance and thus smaller lattice parameter, corresponds to a shift to a higher Raman wavenumber (blue shift), while the reverse corresponds to a lower value (red shift).

X-ray absorption spectroscopy has been commonly used to identify chemical species and oxidation states by interrogating the X-ray absorption near-edge structure (XANES) region. The local bonding environment (e.g., bond length and coordination number) is found in the extended X-ray absorption fine structure (EXAFS) region.¹⁵ For example,

Received: August 25, 2021

Revised: January 14, 2022

Crozier et al.¹⁶ used EXAFS to investigate Br–Mn ion coordination in a $(\text{Br}_4\text{N})\text{MnBr}_3$ melt, showing that the Br–Mn bond length is proportional to the Mn K-edge disorder parameter σ^2 , and provided insight into Mn's locally coordinated structure and coordination numbers. The XAS measurement of molten salts can also be quite challenging since zirconium tetrafluoride-containing systems can form relatively stable glasses and are known for presenting complex behavior in the molten state, where the zirconium coordination number can vary from 5 to 8 and form local complexes ZrF_8^{4-} (coordination number $N = 8$), ZrF_7^{3-} ($N = 7$), ZrF_6^{2-} ($N = 6$), and ZrF_5^- or $\text{Zr}_2\text{F}_{10}^{2-}$ ($N = 5$). For the small alkali atom fluorides LiF and NaF, coordination numbers between 6 and 8 can co-exist below 50 mol % ZrF_4 .^{17–19} For larger alkali atoms (i.e., KF, RbF, and CsF), which are considered as glass progenitors, the coordination of zirconium decreases such that $N = 8$ is not observed in the KF– ZrF_4 system.²⁰ Lower N values result in a phase diagram with a deeper eutectic²¹ than that of LiF or NaF systems. In contrast, SrF_4 with alkali fluorides is known to exhibit a constant $N = 6$ value. A benchmark *in situ* approach is needed to measure coordination numbers in salt melts.

The aim of this research is 2-fold: (1) To demonstrate the efficacy of a novel *in situ* experimental design for Raman spectroscopy and XAS in anticipation of future work on actinide-containing salts and (2) to investigate the coordination environments of a set of two salt melts as benchmarks systems. Specifically, this study investigates the temperature-related effects on the local structure of 1.9 and 5 mol % SrCl_2 in NaCl and 0.8 and 5 mol % ZrF_4 in LiF. The SrCl_2 –NaCl salt is chosen because it does not form ternary compounds and exhibits a single coordination state through the temperature range investigated. The ZrF_4 –LiF salt is known to exhibit more complex behavior as it is expected to form ternary compounds, and the melt's coordination environment of Zr is disordered with multiple Zr–F complexes that can form with different coordination numbers. Chemical speciation and local coordination environments for strontium and zirconium in the salt mixtures were measured using XAS and complemented with calculations using an *ab initio* core-level spectroscopy code, FEFX, to aid in the interpretation of the XANES features. Comparative interpretation of Raman spectra observations was performed using EXAFS bond distance measurements, with FEFX calculations assisting in the fitting of structural data of known compounds with the measured samples.

2. EXPERIMENTAL METHODS

2.1. Sample Preparation. Trace metal grade salts (NaCl, SrCl_2 , LiF, and ZrF_4) were purchased from Sigma-Aldrich: NaCl (99.999%, SKU #204439); SrCl_2 ($\geq 99.99\%$, SKU #439665); LiF ($\geq 99.99\%$, SKU #449903); and ZrF_4 (99.9%, SKU #311464). Prior to spectroscopic measurements of the molten salt samples, their melting points were quantified using differential scanning calorimetry (DSC) with thermogravimetric analysis (TGA). For Raman Spectroscopy, mixtures were prepared from these as 1.9 mol % SrCl_2 in NaCl and 0.8 mol % ZrF_4 in LiF. Figure S1 presents the generalized heat profile representative of those used for DSC and Raman spectroscopy over the measurement temperature range and a view of the Raman *in situ* Linkam high-temperature stage. The heat profile methods used to prepare and to measure the molten salt samples were adapted from Ocadiz-Flores et al.²² and Schreyer et al.²³ for DSC and Raman spectroscopy. Molten salts were

dried, pre-melted, and resolidified during TGA–DSC and subsequently measured using Raman spectroscopy after exposure to the drying heat cycle (Figure S1, middle image). The resulting salts, now termed “pre-melt salts”, were measured with Raman spectroscopy, which accessed molecular vibrational modes and their corresponding wavenumber bands to examine frequency shifts due to composition and temperature changes.

For XAS, unmelted salt mixtures were prepared in the same ratios: 5 mol % SrCl_2 in NaCl and 5 mol % ZrF_4 in LiF. In a glovebag purged with dry N_2 (Airgas NI UHP200) with O_2 content of 1 ppm, the samples were weighed, ground with a mortar & pestle, and loaded using a spatula into pyrolytic boron nitride (BN) sample holders manufactured by QS Advanced Materials (Troy, MI). The BN sample holders used were hot-pressed cylinders 78.2 mm long, with a 12.7 mm deep hole in one end resulting in a 1 mm inner diameter and a 3 mm outer diameter. A BN sample holder was selected because it has good thermal stability up to 1200 °C, was transparent to the X-rays, has low O_2 content of less than 0.07%, and was chemically compatible with the samples. Similar sample holders have been shown to work well for these types of experiments in the past.^{24–26} The samples were packed into the sample holders and then sealed with Aremco Ceramabond 503 (high-temperature, thermally cured AIP adhesive) to affix 3 mm diameter BN discs onto the open ends of the BN tubes. The adhesive was allowed to set at room temperature and subsequently thermally cured as part of *in situ* heating during the experiment. A schematic of the BN sample holder and heater configurations is shown in Figure S2.

2.2. Thermogravimetric Analysis and Differential Scanning Calorimetry. Melting points were measured for the phase-pure molten salts and their salt mixtures with TGA and DSC under continuous argon flow using a Netzsch Simultaneous Thermal Analysis (STA) 449 F3 Jupiter and Proteus data analysis software. Molten salt samples were weighed (semi-microbalance) into specially made 3×7 mm boron nitride (BN) crucibles (Stanford Advanced Materials). The first temperature segment of the generalized heat profile (Figure S1) assures that the salt sample is dehydrated and deoxygenated. The triplet heat cycle assures sample homogeneity and data reproducibility. TGA and DSC curves were calibrated for baseline correction using two empty BN crucibles and a sample's heat profile.

2.3. X-ray Absorption Spectroscopy. This study used a heater that was adapted from a design previously used for *in situ* transmission X-ray experiments.²⁷ The heating element is a modified FibHeater200 from MHI, Inc. (Cincinnati, OH), which is a commercially available MoSi_2 heating element. A water-cooled copper cooling jacket was custom-designed to fit around the heating element and features separate ports for the sample and the X-ray beam. Additionally, a K-type thermocouple was mounted inside the heater assembly to calibrate the sample temperature. The thermocouple was calibrated via a temperature ramp experiment, in which the heater temperature was increased in increments of 200 °C up to the sample melting temperature and then 100 °C up to 1100 °C. After each increment, the temperature inside the heater was recorded as a function of time until it reached a steady state, typically 20–30 min per increment. The temperature response as a function of voltage was fitted to a polynomial, from which the required voltage for each temperature could be predicted. This was necessary because real-time, *in situ*

monitoring of the temperature is not possible using an external thermocouple, while a sample is mounted inside the heater.

The XAS experiments were performed at the Stanford Synchrotron Radiation Lightsource (SSRL), beamline 11-2, as shown in Figure S2. Absorption spectra for the chloride salt mixture were obtained at the Sr K-edge, 16 105.0 eV, and the fluoride salt mixture was obtained at the Zr K-edge, 17 998.0 eV. The XAS spectra were recorded in transmission mode at 25, 200, 400, 600, 700, 800, 900, 1000, and 1100 °C, as well as again at 25 °C after the sample resolidified following the cool-down procedure. At each temperature step, the heater temperature was allowed to equilibrate for 30–40 min. To determine whether BN dilution affects EXAFS data, new samples were prepared in a (1:2) salt/BN molar ratio of 5 mol % ZrF₄ in LiF. X-ray absorption spectra were recorded in transmission mode for the BN-diluted salt at 600 and 1100 °C.

Extraction of EXAFS parameters for the salt samples was carried out using the Demeter software package.²⁸ Fits were obtained up to 1100 °C for the chloride and fluoride salt mixtures. The number of scattering paths used for fitting was verified for statistical significance by a Hamilton F-test.^{29,30} Additional cumulants were added when appropriate to account for anharmonic effects at elevated temperature. The parameters determined by fitting were the coordination number *N*, amplitude reduction factor *S*₀², offset of the absorption peak energy of the data and *E*₀ fit, bond distances between atoms *R*, and the disorder parameter, which factors in thermal and static disorder σ^2 .

Computational EXAFS calculations were carried out for known structures of SrCl₂, ZrF₄, and Zr–Li–F ternary structures using FEFF 9.6.³¹ Each calculation used 2 × 2 × 2 crystal supercell atom clusters. All calculations used an RPA core hole with potentials generated through FEFF using a 4 Å radius and scattering paths were extended out to 8 Å. The maximum half-path used by the simulations was set to 10 Å. These settings were shown to allow calculations to converge for SrCl₂, the smallest crystal modeled. For simplicity, the amplitude factor was set to 1.0 and no thermal corrections were included.

2.4. Raman Spectroscopy. Raman scattering spectroscopy was performed using a Horiba LabRAM HR Evolution Raman microscope, which was equipped with an 800 mm focal length spectrograph, a cooled back-illuminated deep-depleted 1024 × 256 pixels CCD detector, a 100 mW 532 nm laser with no attenuation, a 5× magnification objective, and a diffraction grating of 1800 groves/mm. The Raman microscope, used for initial laser focusing of the sample, provided additional information about the sample morphology, phase state, and particle sizes. Each spectrum was corrected by the pre-recorded instrument-specific response to a calibrated white light source, namely, the intensity correction system. Three or more spectra were obtained for each sample in separate measurements over wavenumber ranges of 80–600 cm for the chlorides and 80–700 cm for the fluorides. Each spectrum consists of an average of ten 15 s long scans. Samples were measured under a continuous argon atmosphere (55 cm³/min) over 25–1000 °C, using a TS1500 Linkam stage and an associated T96 System Controller (±0.1 °C set point resolution) to control the applied heat profile (Figure S1, middle image). After completion of DSC, sample pre-melts were transported still in their 3 × 7 mm BN crucibles having been secured in a plastic box with a snap-close gasket seal to the Raman spectroscopy suite, transferred into the Linkam heat stage, and then redried/

degassed to ensure that adventitious water and oxygen were not present in the sample using the heat profile program schema of Figure S1 (middle image). Continuous water circulation through the Linkam stage allowed for regulated cooling, while the heating element controlled the absolute temperature, both of which were monitored with an internal thermocouple. The T96 System Controller sensor is a type-S Pt-10% Rh/Pt thermocouple. A sapphire disc makes contact between the sample crucible and the thermocouple to confirm an accurate temperature measurement from the sample.

3. RESULTS AND DISCUSSION

3.1. Thermogravimetric Analysis and Differential Scanning Calorimetry. Table 1 presents sample composi-

Table 1. Molten Salt Composition and TGA–DSC Melting Point Comparisons between the Literature and This Work

molten salts	melting point (°C) from ref 34	measured melting point (°C)	FactSage computed melting point (°C)
SrCl ₂	874	874.0 ± 0.5	874 ± 1
NaCl	801	801.0 ± 0.5	801 ± 1
1.9 mol % SrCl ₂ /NaCl	^a	795.5 ± 0.5	794 ± 2
5 mol % SrCl ₂ /NaCl	^a		782 ± 2
ZrF ₄	910	910.0 ± 0.5	907 ± 5 ^b
LiF	848	848.0 ± 0.5	846 ± 1
0.8 mol % ZrF ₄ /LiF	^a	843.0 ± 0.5	843 ± 5
5 mol % ZrF ₄ /LiF	^a		824 ± 5

^aNo published values. ^bSublimation temperature.

tions and melting point data (published and measured values). Errors are ±0.5 °C for the average of three measurements. For the phase-pure molten salt samples, there is good agreement between available published values⁹ and measurements from the present work, suggesting phase-pure compounds. Melting points for the salt mixtures do not have available published values for comparison. Melting points predicted using FactSage 8.1³² with the MSTDB database³³ software agree well with measurements.

3.2. X-ray Absorption Spectroscopy. **3.2.1. X-ray Absorption Near-Edge Structure (XANES) Region.** The X-ray absorption near-edge structure for salt mixtures with 5 mol % SrCl₂ in NaCl and 5 mol % ZrF₄ in LiF at room temperature (25 °C) compares well to absorption spectra computed by FEFF (Figure 1), which serves to verify our experimental measurements. The XANES spectra for the chloride and fluoride salt mixtures at different temperatures shown in Figure 2 are consistent with the literature.^{35,36} Two scans in Figure 2a at 1100 and 25 °C after resolidification warrant further inspection due to their unique features compared to the other spectra. A comparison of the 1100, 25, and the 1000 °C spectra shows a new peak at $\sim E_0 + 10$ eV, a valley at $E_0 + 18$ eV (in the other scans, there is a peak at this location), and a slight peak at $E_0 + 36$ eV, which rises at a lower energy than in the other scans. Qualitatively, these features resemble those observed by D'Angelo et al.³⁷ in hydrated Sr systems, [Sr(H₂O)₈](OH)₂, which may suggest that the Sr in the 1100 and 25 °C post resolidification scans are hydrated as well. This could either be due to environmental contamination during the experiment or due to water evaporation from the Aremco Ceramabond 503 adhesive used to seal the BN sample holders. The Zr K-edge XANES spectra for fluoride salt

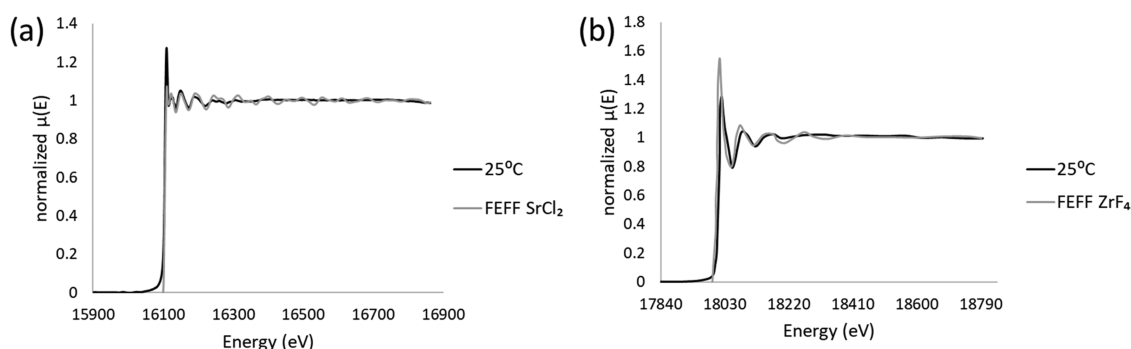


Figure 1. Comparison of experimental normalized $\mu(E)$ obtained by XAFS to FEFF predictions for (a) 5 mol % SrCl_2 in the NaCl salt mixture and (b) 5 mol % ZrF_4 in the LiF salt mixture.

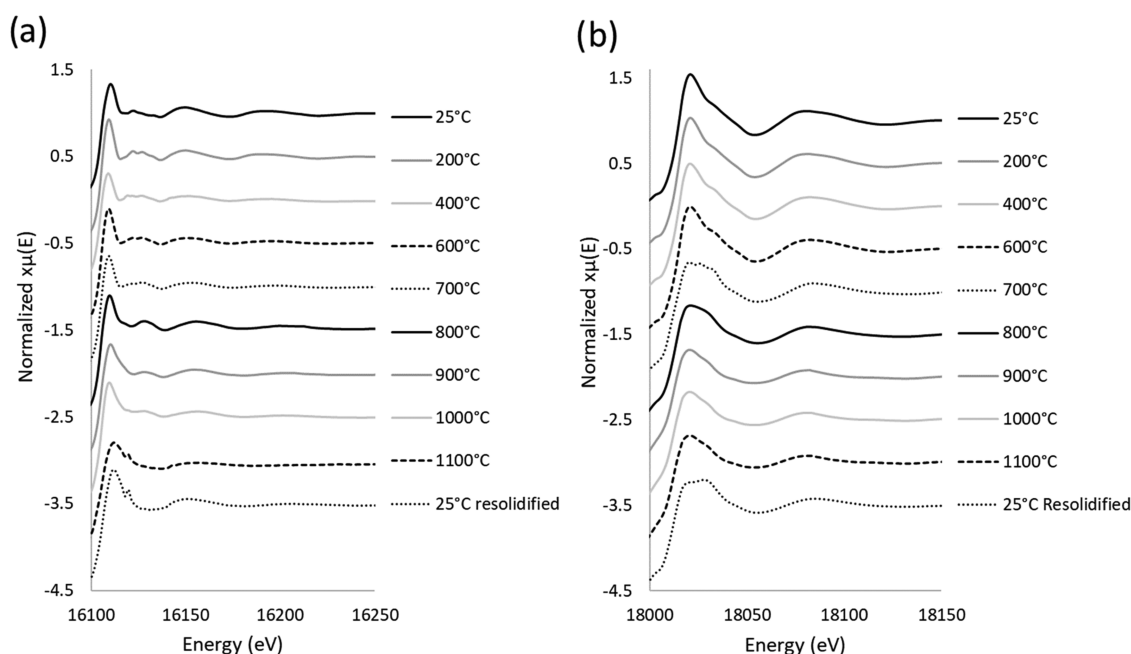


Figure 2. Normalized XANES for (a) 5 mol % SrCl_2 in NaCl chloride salts (recorded across the Sr K-edge, 16 105 eV) and (b) 5 mol % ZrF_4 in LiF fluoride salts (recorded across the Zr K-edge, 17 998 eV). Spectra are normalized and offset for clarity.

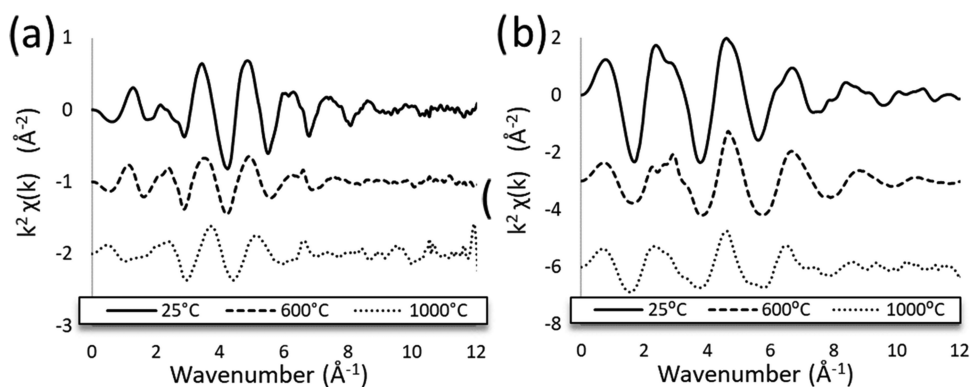


Figure 3. EXAFS oscillations ($k^2\chi(k)$) in k -space for (a) 5 mol % SrCl_2 in the NaCl chloride salt mixture (recorded across the Sr K-edge) and (b) 5 mol % ZrF_4 in the LiF fluoride salt mixture (recorded across the Zr K-edge).

mixtures at elevated temperature show a splitting of the white line, which can be attributed to a change in the first shell coordination number.^{38,39} This suggests that multiple Zr coordination complexes may exist in the fluoride salt mixture.

3.2.2. Extended X-ray Absorption Fine Structure (XANES) Region. The k^2 -weighted oscillations in the EXAFS spectra for

chloride and fluoride salts at selected temperatures (25, 600, and 1100 °C) are shown in Figure 3. In general, the effect of increasing the temperature is to decrease the amplitude and number of the oscillations in k -space. It is known that the elevated temperature also results in asymmetry and spreading of the radial distribution function due to anharmonic

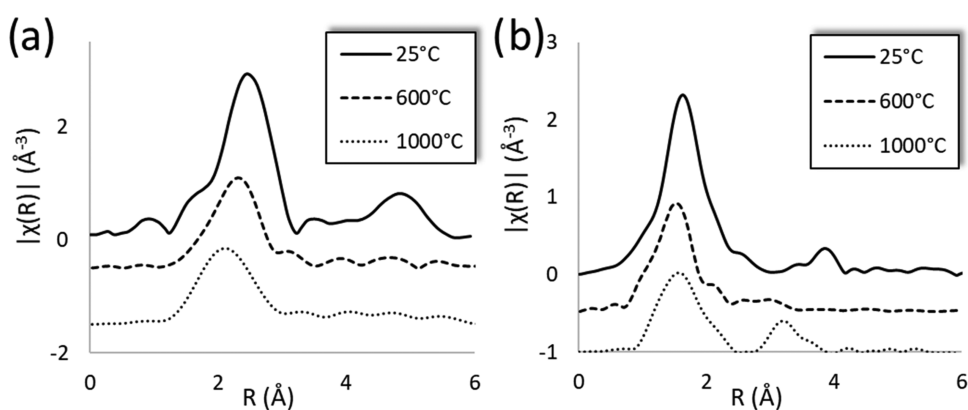


Figure 4. Fourier transform magnitudes of the EXAFS oscillations for (a) 5 mol % SrCl_2 in the NaCl salt mixture (recorded across the Sr K-edge) and (b) 5 mol % ZrF_4 in the LiF salt mixture (recorded across the Zr K-edge). The k -ranges for the Fourier transforms for the chloride salts are listed in Table S3. The fluoride salt k -ranges for the Fourier transforms are all 3–10 \AA^{-1} .

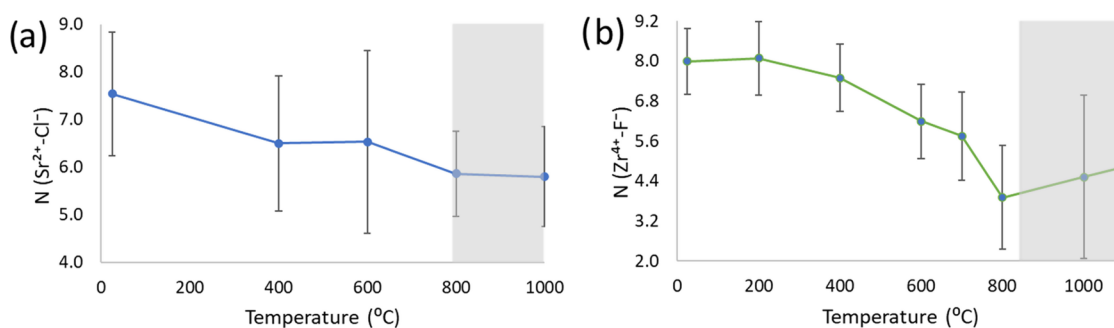


Figure 5. Measured coordination number of the Sr and Zr first shell with temperature for (a) 5 mol % SrCl_2 in NaCl and (b) 5 mol % ZrF_4 in LiF. Tabulated data of all EXAFS parameters are shown in Tables S1 and S2. The melt region is shaded in gray.

vibrations. One example of this can be seen in Figure S3 for the 1000 °C R-space. These features are confirmed by conducting multiple experiments at increasing temperature steps and tracking the EXAFS fitting parameters that will be most prominently affected by the thermal disorder, namely, the disorder parameter σ^2 associated with atom vibration and the interatomic distance due to thermal disorder and additional cumulants.

The molten chloride salt mixture in Figure 4a (at 1000 °C) shows a clear first nearest-neighbor peak with no discernable longer-range order. Like the chloride salt, the peaks in the fluoride salt shift to shorter distances at higher temperature, reducing the liquid-state first nearest neighbor to 1.53 Å. The Fourier transform of the 25 °C ZrF_4 oscillations, Figure 4b, shows two predominate peaks at 1.69 and 3.80 Å, which agree with the structure obtained by Bessada and co-workers.^{25,26} However, the molten fluoride salt mixture, Figure 4b, exhibits a peak at ~ 3.37 Å, which was not observed by Bessada et al.⁴⁰ for similar material systems. Bessada et al. studied high zirconium concentration salt mixtures (15–85 mol % ZrF_4 –KF) that were melted and then resolidified to form a single ternary compound but only heated the sample up to 700 °C. Therefore, it is possible that we observed a different structure due to physical, real differences in the systems, and that the salt mixture was not pre-melted. Our samples span regions of the ZrF_4 –LiF phase diagram where ZrF_4 undergoes a polymorphic transformation from α to β and can also form the Li_3ZrF_7 ternary structure. Unfortunately, phase transformation of ZrF_4 (s) was not reported by Grande et al.,⁴¹ and there exists

no complete crystallographic data for Li_3ZrF_7 to verify this phase transformation with FEFF calculations.

A SrCl_2 crystal⁴² is used to calculate the EXAFS parameters for 5 mol % SrCl_2 in NaCl. Depending on data quality, different k -ranges listed in Table S3 are used to calculate the Fourier transforms shown in Figure S3. FEFF calculations in Artemis determined the best scattering paths with corresponding bond lengths that are close to Okamoto et al.³⁵ The first shell of the data is fitted using the third cumulants³⁵ to account for anharmonic effects at high temperatures, namely, at 800 and 1000 °C. All fits are confirmed to meet the Nyquist criterion. The calculated first shell (Sr^{2+} – Cl^-) coordination number is shown in Figure 5a. As expected, the coordination of its first shell decreases with the temperature, with coordination number $N = 7.5 \pm 1.3$ at 25 °C decreasing to 5.8 ± 1.1 at 1000 °C. The complete set of fitted EXAFS parameters in Table S1 shows some agreement with Okamoto et al.,³⁵ where the parameters at 25 °C match well.

EXAFS parameters for 5 mol % ZrF_4 in LiF are calculated using a reported structure of ZrF_4 .⁴³ Depending on data quality, different k -ranges listed in Table S4 are used to calculate the Fourier transforms shown in Figure S6 and followed similar fitting criteria as the chloride salts. The calculated first shell (Zr^{4+} – F^-) coordination number for the fluoride salt is shown in Figure 5b and the complete set of fitted EXAFS parameters is shown in Table S2. A first shell distance of 2.01 Å shows agreement with Pauvert et al.¹¹ Anomalously, low N is measured at elevated temperature, which is probably due to a distortion of the absorption spectra caused by interference from multiple Zr complexes with

Table 2. Frequency Bands (ν/cm) and Vibrational Modes of 1.9 mol % $SrCl_2$ in NaCl

ν/cm , $T_{25} \text{ } ^\circ\text{C}$, literature values	mode	ν/cm , $T_{25} \text{ } ^\circ\text{C}^a$	ν/cm , $T_{200} \text{ } ^\circ\text{C}^a$	ν/cm , $T_{400} \text{ } ^\circ\text{C}^a$	ν/cm , T_{MP}^a
none reported	T_{2g}	182	178	172	none

^aThis work. Literature value modes were reported as $\nu(25 \text{ } ^\circ\text{C})$.

different coordination numbers in the melt, as further discussed below. As expected, the coordination number decreases with the temperature, while the disorder parameter σ^2 increases with the temperature overall.

3.2.3. Zr–Li–F Ternary Compounds. At room temperature ($25 \text{ } ^\circ\text{C}$), ZrF_4 is expected to have a tetragonal structure with $N = 8$. As the temperature is increased beyond $474 \pm 5 \text{ } ^\circ\text{C}$, Li_3ZrF_7 is expected to form.²¹ The possible formation of Li_3ZrF_7 ternary complicated the analysis of XAS spectra above $600 \text{ } ^\circ\text{C}$ for two reasons: (1) The literature shows disagreement between authors who have studied Li_3ZrF_7 . Brunton et al.⁴⁴ published unindexed X-ray patterns for α and β Li_3ZrF_7 . Two-phase diagrams have been published^{21,45} around the same time, showing agreement about the dimorphism of Li_3ZrF_7 , however, with very different temperatures of transition. Later, Dugat et al.⁴⁶ revisited the LiF – ZrF_4 system and concluded that the indexed X-ray patterns of the Li_4ZrF_8 phases are very similar to that given for β - Li_3ZrF_7 . (2) Complete crystallographic data is not available for α and β - Li_3ZrF_7 structures. Only partial data is available, such as unindexed X-ray patterns,⁴⁴ and unit cell parameters are published by a project at the National Science Center Kharkiv Institute of Physics and Technology⁴⁷ where they indexed a crystallographic structure for Li_3ZrF_7 using these X-ray patterns.

A comparison of simulated EXAFS for three different ternaries (Li_2ZrF_6 , $Li_3Zr_4F_{19}$, Li_4ZrF_8) at $1000 \text{ } ^\circ\text{C}$ was performed in Figure S4 to demonstrate probable ternary formation with the fitted disorder parameters shown in Table S2. The resolidified 5% ZrF_4 in the LiF salt mixture in Figure S5 shows a qualitative match with a FEFF generated R-space and k -space for Li_4ZrF_8 , which at the given mixture concentrations shows agreement with Beneš et al.⁴⁸ Since the samples qualitatively match up with FEFF generated ternary spectra, it is probable that a ternary formed in the fluoride sample. However, this cannot be confirmed because there is limited information for Li_3ZrF_7 .

The value of coordination number is anomalously low at and above the melting temperature of the 5 mol % ZrF_4 in LiF . Figure 5b demonstrates this at and above $800 \text{ } ^\circ\text{C}$. These values may not represent the actual coordination number of the melt at these temperatures due to the presence of multiple complexes ($N = 6$ – 8) that is expected to create destructive interference in the absorption spectra. Molecular dynamic simulations using an interaction potential derived from the polarizable ion model predicted an average coordination number of $N = 7 \pm 0.07$ for 5 mol % ZrF_4 in LiF at 50 K above the melting point.¹⁷ We believe that this difference may be induced by the presence of multiple complexes ZrF_6^{2-} , ZrF_7^{3-} , and ZrF_8^{4-} that create their own EXAFS spectra. In the molten state, the fluoride salt is expected to have a coexistence of three different Zr-based complexes, ZrF_6^{2-} , ZrF_7^{3-} , and ZrF_8^{4-} , where zirconium is 6, 7, and 8 coordinated by fluorine, respectively.^{11,17} At much higher zirconium concentration near deep eutectics, ZrF_5^- with $N = 5$ can also be present,¹⁹ but this species is not expected to be present in the current study. Since literature has reported the formation of ternary compounds and a disordered coordination environment of zirconium in the

molten state, we expect some potential challenges in measuring the local coordination around Zr^{4+} . The measured EXAFS spectra are an averaged spectrum that can be distorted due to interference between the spectra of the individual complexes. A similar situation was recently reported by Gill et al.,⁶ where the coordination environment of Ni(II) in $ZnCl_2$ is disordered among tetra- and pentacoordinate states, resulting in anomalously low Ni(II) coordination numbers in the melt. The especially low $800 \text{ } ^\circ\text{C}$ coordination number sits near a solid/liquid phase boundary in the Zr–Li–F phase diagram,⁴⁶ which could also help to further contribute to a lower coordination number due to possible resolidification of the melt.

3.2.4. Boron Nitride Powder Dilution. The XAS measurement of actinide-containing salts can also be quite challenging due to significantly noticeable attenuation in the transmitted X-ray intensity. To circumvent this issue, researchers have used BN powder as a salt diluent.^{25,26} However, it was unclear if such a diluent will interfere with the measurement. A benchmark study to determine if BN can potentially modify the local coordination of ions in the melt will provide a deeper understanding of the use of BN powder as a salt diluent. Figure S11 shows BN powder as a sample diluent for the 5 mol % ZrF_4 in the LiF fluoride salt mixture with a 2:1 BN powder to salt mixture ratio. The BN powder used has a median particle size of $7.4 \mu\text{m}$ and an O_2 content of 0.58% (ZYP Coatings, Inc., Oak Ridge, TN). The BN-diluted samples at $600 \text{ } ^\circ\text{C}$ were compared to a nondiluted sample across the Zr K-edge in Figure S11. Figure S11a,b shows a negligible effect of BN in energy space. Likewise, Figure S11c shows that the local coordination environment remains unchanged. Therefore, BN powder shows promise as a diluent for future EXAFS experiments on similar salt mixtures.

3.3. Raman Spectroscopy. **3.3.1. 1.9 mol % $SrCl_2$ in the NaCl Salt Mixture.** There are no previous reports of vibrational frequencies of 1.9 mol % $SrCl_2$ in NaCl. Frequencies and corresponding vibrational modes measured at 25, 200, 400 $^\circ\text{C}$, and the melting point ($796 \text{ } ^\circ\text{C}$) are shown in Table 2 with the Raman spectra in Figure 6. Measured at $25 \text{ } ^\circ\text{C}$, the single observable band at 182 cm is for the T_{2g} mode, which is comparable to pure $SrCl_2$ (179 cm). The Raman band correlates well within experimental error with that measured by Schreyer et al.²³ after annealing the $SrCl_2$ sample at $400 \text{ } ^\circ\text{C}$ for 10 min ($\nu = 181.5 \pm 1 \text{ cm}$). This too agreed well with that reported by a number of investigators.^{49–52} A blue shift by a few wavenumbers suggests, relative to the $SrCl_2$ structure, that the $25 \text{ } ^\circ\text{C}$ pre-melt Cl-mix solid has a decreased lattice parameter or compressed structure. Additionally, at all temperatures below the MP for this Cl-mix, the only observable band is assignable to the higher valent cation component, $SrCl_2$. With increasing temperature, this band red shifts (to a lower frequency). The decreased frequency may correlate with the bond length increase (loosely interpreted as bond weakening or structure expansion). Frequencies are not evident above the melting point temperature.

The major source of light scattering in the visible and the near-ultraviolet is the electronic cloud of the molecules (not

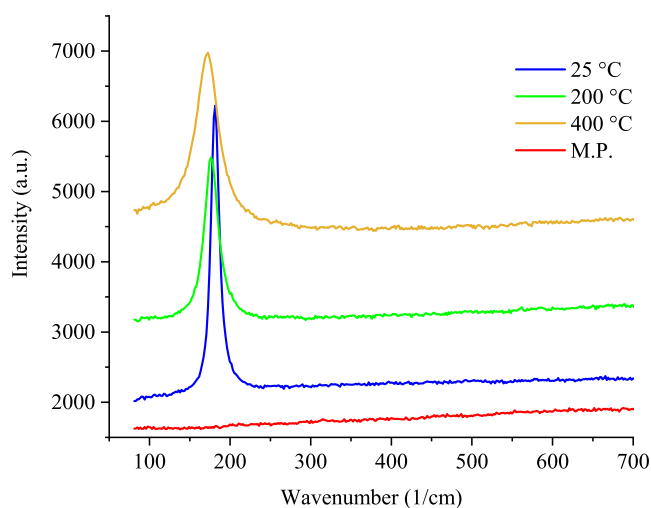


Figure 6. Raman spectra of 1.9 mol % $\text{SrCl}_2/\text{NaCl}$ at 25, 200, 400 °C, and melting point (796 °C).

the nuclei).⁵³ Raman spectroscopy is based on the Raman inelastic scattering mechanism in which a molecule is induced to oscillate by the incident electromagnetic radiation. The resulting dipole moment, or oscillating molecular/electronic polarizability, gives rise to the measured intensity of the scattered radiation as a function of this polarizability (ref 54, pg. 164, and detailed in eq 6.9 therein). As we are studying molten salts, important effects influence electronic polarizability, namely, the group 1 and 2 metal cations and the relatively huge halide anions. Anion–anion polarization fluctuation enhances isotropic light scattering and corresponds with an increased number of phonon frequency interactions with the incident beam. Although the volume occupied by the cation electron density of strontium is larger than that of sodium, strontium content in the Cl-mixture is very small. Additionally, due to the small size of sodium, chloride electron density clouds are essentially proximal in the Cl-mixture comprised of a large population of NaCl (98.1 mol %). Thus, in the Cl-mixture, relative to a purely SrCl_2 sample, the development of an intense symmetric field can occur about the Cl anions with minimal anisotropic dipole-induced-dipole interference from strontium.⁵³ The results are increased energy of the emitted scattered light and a corresponding blue shift. Thus, NaCl assists in the blue shift observed in the Cl-mixture spectra.

3.3.2. 0.8 mol % ZrF_4 in the LiF Salt Mixture. Vibrational frequencies for 0.8 mol % ZrF_4 in LiF have not been previously reported. Frequency bands are compared with those from the literature in Table 3 with the Raman spectra in Figure 7. Our 0.8 mol % ZrF_4 in LiF mix and pure ZrF_4 Raman spectra have

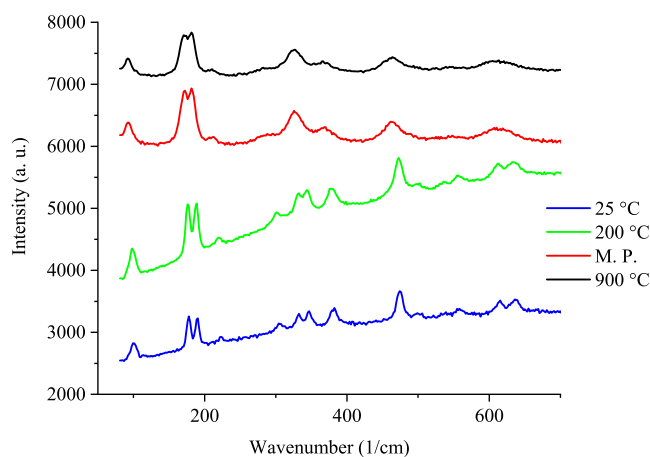


Figure 7. Raman spectra of 0.8 mol % ZrF_4/LiF at 25, 200 °C, melting point (843 °C), and 900 °C.

characteristics much like that of $\beta\text{-BaZrF}_6$, which is an $N = 8$ Zr representative fluorozirconate solid phase.⁵⁵ The intense symmetric modes (Table 3) of our solid phase 0.8 mol % ZrF_4 in LiF transferred to the molten phase, which included 178–190 cm (split peak, sp), 333–347 cm (split peak), 371–398, and 467–481 cm, with ν_s at 553–565 cm. The splitting relates to the Zr in a site of lower symmetry (breaking symmetry).⁵⁶ Because the ν_s (symmetric Zr–F stretching vibration of nonbridging, terminal Zr–F bonds) and the frequencies for all symmetric mode vibrations (symmetric Zr–F stretching or bending) were translated from the solid to melt phase and the spectra present with similar characteristics as that of the Zr $N = 8$ representative solid phase, $\beta\text{-BaZrF}_6$,⁵⁵ suggests that this is the coordination geometry of our 0.8 mol % ZrF_4 in the LiF sample in the melt. The purpose of using alkali- or alkaline-rich fluoride in the fluoride salt mixture is to diminish the formation of F-linkages.⁵⁶ Only in the absence of F-bridging with Zr, does an inverse correlation exist between the high-frequency symmetric Zr–F stretching band of nonbridging, terminal Zr–F bonds (ν_s) and the Zr coordination number.^{56,57} Thus, only isolated ZrF_n^{4-n} units should be present in the melt and relate directly to the Zr coordination environment.

However, vibrational bands may not be directly correlated between the ν_s and the F-coordination number of Zr in our mixture with the alkali or alkaline fluorozirconates in the literature. This may be due to a current gap in the art for attributing the ν_s and the F–Zr coordination number in fluorozirconates. The ν_s of representative fluorozirconate solid-phase structures, even at constant Zr $N = 8$, can exhibit a significantly lower coordination number in the melt. For

Table 3. Frequency Bands (ν/cm) and Assignments of 0.8 mol % ZrF_4 in LiF

ν/cm , $T_{25} \text{ } ^\circ\text{C}^{\text{b}}$	assignment	ν/cm , $T_{25} \text{ } ^\circ\text{C}^{\text{a}}$	ν/cm , $T_{200} \text{ } ^\circ\text{C}^{\text{a}}$	ν/cm , T_{MP}^{a}
568–591 ^b	symmetric Zr–F stretching, $N = 8$	553–565	551–565	542–558
472–486 ^c	Zr–F stretching and F-bridging	467–481	465–479	451–478
385–400 ^c	Zr–F stretching and F-bridging	371–398	368–397	358–380
330–350 ^c	Zr–F stretching and F-bridging	333–347 (sp)	332–345 (sp)	317–339
180–190 ^d	bending modes	178–190 (sp)	176–189 (sp)	172–181 (sp)

^aThis work. The literature values are reported as $\nu(25 \text{ } ^\circ\text{C})^{\text{b}}$ for measured ternary systems of zirconate glasses. Assignments: ^bSymmetric Zr–F stretching vibration of nonbridging, terminal Zr–F bonds assigned as the ν_s ; ^cSymmetric Zr–F stretching also involved in Zr–F–Zr linkages; ^dF–Zr–F or Zr–F–Zr bending modes. Split peak is denoted (sp).

instance, ν_s for the representative Zr $N = 8$ solid-phase structure, K_2ZrF_6 , is found at 525 cm⁻¹ ($F/Zr = 6$) at 25 °C. Comparatively, for the solid phases of β -BaZrF₆, α -PbZrF₆, and α -SrZrF₆, ν_s correspond as 562, 567, and 578, respectively.⁵⁵ These differences are speculated⁵⁵ to be related to the Badger rule,⁵⁹ which correlates an inverse relationship between ν_s and F–Zr bond length and as such the band would shift accordingly (e.g., blue shift for shorter bond length). Additionally, the F/Zr ratio affects the ν_s frequency. Toth and co-workers⁵⁶ added alkali metal fluorides (LiF–NaF) to change the ZrF₄ concentration in fluorozirconate melts, which resulted in the ν_s symmetric stretching vibration to shift accordingly, 40 mol % (593 cm⁻¹), 33 mol % (577 cm⁻¹) to 20 mol % (555 cm⁻¹). Contributing to this complexity, F-bridging also influences the F–Zr bond length of terminal M–X bonds, which consequently are correlated specifically with ν_s .⁵⁷ Essentially, ν_s increases with the decreased F/Zr ratio, decreased counter cation radius, decreased Zr coordination number, increased counter cation coordination number, and increased F-bridging.

Solid-phase Zr(IV)F₄ is polymorphic with eight F ions shared between neighboring Zr(IV) cations forming compact ZrF₈ triangular dodecahedra structures.⁴³ Raman spectra studies of polymorphic Zr(IV)F₄ structures with Zr $N = 8$ have demonstrated translation of Zr–F symmetric mode vibrations into the melt, with the Zr remaining 8-fold coordinated by F. Such structures previously studied include β -BaZrF₆, α -PbZrF₆, and α -SrZrF₆ for which it was proposed that the basic structures in the melt were chains of ZrF₈ dodecahedra.⁵⁵ However, it has been suggested that an 8-fold coordinated Zr crystalline structure can exist in a significantly lower coordination number in the melt, due to a large entropy of fusion.⁵⁸ Indeed, it has been previously reported that the ν_s frequency observed for melts at a constant F/Zr ratio blue shifted to significantly higher frequencies than that of solid-phase fluorozirconates, due to configurational changes that decreased the Zr coordination number with heating above the glass transition temperature.⁵⁸ If such structural changes did not occur with transformation to the melt, then ν_s frequency should decrease, due to thermal expansion and anharmonic effects.^{58,60}

With the decreased F/Zr ratio (e.g., ZrF₄ content increase), the ν_s frequency increases (blue shift) significantly upon melting due to the decreased Zr coordination number.^{56–58} However, others have reported that the Zr coordination number increases with the decreased F/Zr ratio.^{61,62} Further, with a decrease in the F/Zr ratio, increasing ν_s frequency has been observed due to increased F-bridging between ZrF_{*n*} polyhedra. Toth and co-workers⁵⁶ reported a similar frequency increase as corresponding to network formation in the melt from increased F-bridging between ZrF_{*n*} polyhedral. The symmetric stretching vibration should increase with the occurrence of F-bridging based on the premise that the formation of a bridged species causes a decrease in the bond order of the individual bonds and thus a decrease in their force constants.^{56,57} In other words, the frequency blue shift is due to the replacement of terminal M–F bonds by M–F–M bridging bonds causing the electron density to shift from M to the remaining M–F terminal bonds, which are then shortened.⁵⁷ Indeed, a general trend for some Zr ($N = 8$) isostructural crystals, (e.g., β -BaZrF₆, α -SrZrF₆, and α -PbZrF₆), correlates increased ν_s frequency (high-frequency band correlated with the symmetric Zr–F stretching mode) with

decreased terminal Zr–F bond length.^{57,59,63} Thus, increased F-bridging as well as decreased Zr coordination number would be expected to blue shift the high-frequency band (ν_s) in the melt.

Complicating matters are the issue that F-bridging is quite fragile in fluorozirconate systems and as such with temperature increase, particularly above the glass transition temperature where these linkages are readily susceptible to dissociation.^{56,57,64} The effect of fewer bridging X–M–X bonds is the lengthening of terminal X–M bonds, which correlates with decreased vibrational frequency. As the symmetric stretching bands in our very high F/Zr ratio mixture did not blue shift as they translated from the solid into the melt, we must surmise that the coordination number of Zr did not decrease in the melt or that the F-bridging at elevated temperature is too fragile and may subsequently decompose. Without a crystal structure with which to make a direct comparison, it will be impossible to speculate what the actual coordination number is for the Zr without risking over the interpretation of our data. Additional studies are in progress to address these issues. That being said, a logical and educated hypothesis can be made as presented here. This is stated as a caveat to use multiple sources of information to make this assignment firmly. This is currently being done with phonon calculations in our next work.

3.4. Comparison of X-ray Absorption Spectroscopy and Raman Spectroscopy Measurements. The chloride salt mixture exhibits vibrational modes that are consistent with the literature.^{65–67} The chloride mix Raman spectra present only one frequency band, which is common to that of pure SrCl₂. The Raman bands of both salt mixtures studied initially blue shift relative to the pure salt at room temperature. The bands then red shift to a lower frequency with an increase in the temperature, which is consistent with a decrease in bond length measured by EXAFS.

Polymorphs of crystalline Zr(IV)F₄ share eight F ions between neighboring Zr(IV) cations, which form ZrF₈ triangular dodecahedra structures.⁴³ Raman studies of such structures demonstrate translation of the intense high-frequency symmetric band (ν_s) corresponding with the Zr–F stretching vibrational mode from the solid phase into the melt, with the Zr remaining 8-fold coordinated by F. This has been shown in a number of structures previously studied including β -BaZrF₆, α -PbZrF₆, and α -SrZrF₆.⁵⁵ Indeed, in the absence of F-bridging, all intense symmetric modes of the solid are transferred into the melt such that isolated geometries (e.g., ZrF_{*n*}^{4–*n*} units) are identifiable and correlate with the Zr–F-coordination number of the crystalline structure.

Our fluoride mixture retains the character of the pure ZrF₄ spectra, which has characteristics similar to the Zr $N = 8$ alkaline earth fluorozirconate, β -BaZrF₆.⁵⁵ The intense ν_s (symmetric Zr–F stretching vibration of nonbridging, terminal Zr–F bonds) and all symmetric modes (symmetric Zr–F stretching or bending), present at 25 °C in the solid phase, translate to the melt with a red shift of all vibrational bands to lower wavenumbers. Both local structures have also been suggested by EXAFS measurements as part of the coexistence of multiple Zr-based complexes in the fluoride melt.

This does not initially seem consistent with a decrease in the first nearest-neighbor bond length measured in EXAFS. The reason for this is that the relationship is complex. Essentially, with increasing temperature, the observed decrease in the frequency of the ν_s band as well as the frequencies for all

symmetric modes is due to the very high F/Zr ratio. This is related to structural changes involving decreased Zr coordination number and increased F-bridging. Only in the absence of F-bridging with Zr, does an inverse correlation exist between the ν_s and the Zr coordination number. Conversely, increased F-bridging increases the F–Zr bond length of terminal M–X bonds, which are also correlated with ν_s . The symmetric stretching vibration should decrease (red-shift) with the occurrence of F-bridging and is based on the premise that formation of a bridged species decreases the bond order of the individual bonds with a corresponding decrease in their force constants. F-bridging is also quite fragile in fluorozirconate systems, and as such with the temperature increase above the glass transition, these linkages are readily susceptible to dissociation. Thus, in the melt, a system complexed with perhaps a number of ion species with transient F-bridging and formation of local networks of a higher coordination number then dissociates to a decreased coordination number. This may account for the development of Zr species with low coordination numbers and explain why there is an extensive broadening of the frequencies that are correlated specifically with the symmetric modes related to both symmetric Zr–F stretching also involved in Zr–F–Zr linkages as well as the symmetric Zr–F stretching vibration of nonbridging, terminal Zr–F bonds assigned as the ν_s . When F-bridging occurs in the solid phase, the frequencies of the vibrational modes cannot be predicted accurately. Alkali metal fluoride was present in large excess in this study to minimize fluoride ion bridging between zirconium-containing complex ions in the melt. Therefore, the F-mix spectra of the melt are presumed to arise from a free ZrF_x^{4-z} species.

4. CONCLUSIONS

In this work, the local structures of strontium in a 1.9 and 5 mol % $SrCl_2$ –NaCl melt and zirconium in a 0.8 and 5 mol % ZrF_4 –LiF melt were investigated as a proof-of-concept study using techniques that will be applied to more challenging actinide salts. The efforts included studies of the crystalline phases and melt from room temperature to 1100 °C via *in situ* XAS spectroscopy supported by *ab initio* FEFF calculations and Raman spectroscopy, focusing on the near-edge XANES and extended fine structure EXAFS of the X-ray absorption spectra.

The 1.9 and 5 mol % $SrCl_2$ –NaCl melt is an ideal salt mixture for Raman spectroscopy and XAS spectroscopy, respectively, because it did not form ternary compounds and exhibited a single coordination state through the temperature range investigated. It was observed that strontium is coordinated by chlorine, with the (Sr^{2+} – Cl^-) coordination number decreased from $N = 7.5 \pm 1.3$ at 25 °C to $N = 5.8 \pm 1.1$ at 1000 °C. This chloride salt mixture presents only one Raman frequency band, which is common to that of pure $SrCl_2$. The Raman band initially blue shifts relative to the pure salt at room temperature and then red shifts to a lower frequency with increasing temperature, which is consistent with a decrease in bond length measured by EXAFS.

Zirconium coordination is known to exhibit more complex behavior than that of strontium in the systems investigated. The current measurements indicated that zirconium behaves in a manner analogous to that of the chloride where the first shell is coordinated by fluorine such that the (Zr^{4+} – F^-) coordination number decreases with the temperature. At room temperature (25 °C), ZrF_4 is observed to have a

tetragonal structure with $N = 8$. However, as the temperature is increased beyond 487 °C, ternary formation significantly complicates the analysis. It appears that the melt contains multiple complexes consisting of ZrF_6^{2-} , ZrF_7^{3-} , and ZrF_8^{4-} where zirconium is in a 6, 7, or 8 coordination with fluorine, respectively. Our measured EXAFS spectra are thus average spectra that can be distorted due to interference between the spectra provided by each of the individual complexes.

The Raman spectra obtained for the systems studied here agree with those previously reported for the F/Zr ratios yielding the resultant vibrational frequency shifts. Frequencies are seen to decrease with the increasing F/Zr ratio in the fluoride salt mixture. Additionally, the very high F/Zr ratio of our 0.8 and 5 mol % ZrF_4 in LiF essentially drives the system to develop isolated ZrF_n^{4-n} units and in this case units of ZrF_8 . In addition, F–Zr–F-bridging is seen to be fragile and thus sensitive to the concentration of alkali or alkaline cation content as well as elevated temperature. Hence, a crystalline structure with 8-fold coordinated zirconium can exhibit a significantly lower N value in the melt due to a large entropy of fusion.

The use of BN powder as a salt diluent for XAFS measurements, important for future measurements with actinide-containing salts that noticeably attenuate the transmitted X-ray intensity, was found to not interfere with measurements and thus can be used for XAFS investigations of such systems.

Overall, the approaches described here for *in situ* investigations of salt melt local structure have been successful. Salt systems without complex ternary formation such as the $SrCl_2$ –NaCl system can be readily studied by XAFS and Raman spectroscopy. However, the complex ZrF_4 –LiF system that forms complex ternary compounds presents additional challenges but proved particularly apt for illustrating the methodologies that will be next applied to actinide salt melts to help understand their known multitude of local structures.

■ ASSOCIATED CONTENT

SI Supporting Information

The Supporting Information is available free of charge at <https://pubs.acs.org/doi/10.1021/acs.jpcb.1c07552>.

Calculated EXAFS parameters and *k*-range and *R*-range window used for Fourier transforms to *R*-space for the 5 mol % $SrCl_2$ –NaCl salt mixture and the 5 mol % ZrF_4 –LiF salt mixture; experimental details for DSC, Raman, and X-ray absorption spectroscopy measurements; *R*-space, *k*-space, and $Im[R]$ fits for the salt mixtures; comparison of FEFF calculated to EXAFS measurements for Li–Zr–F ternary compounds, resolidified 5% ZrF_4 in LiF and ZrF_4 –LiF salt mixtures with boron nitride dilution (PDF)

■ AUTHOR INFORMATION

Corresponding Author

Wilson K. S. Chiu – Department of Mechanical Engineering, University of Connecticut, Storrs, Connecticut 06369-3139, United States; orcid.org/0000-0001-7402-4951; Email: wchiu@engr.uconn.edu

Authors

Timothy J. Lynch – Department of Mechanical Engineering, University of Connecticut, Storrs, Connecticut 06369-3139, United States

Nancy R. Birkner – Department of Materials Science and Engineering, Clemson University, Clemson, South Carolina 29634-0901, United States

Matthew S. Christian – Nuclear Engineering Program, University of South Carolina, Columbia, South Carolina 29208, United States; orcid.org/0000-0002-3416-413X

Jacob A. Wrubel – Department of Mechanical Engineering, University of Connecticut, Storrs, Connecticut 06369-3139, United States

Juliano Schorne-Pinto – Nuclear Engineering Program, University of South Carolina, Columbia, South Carolina 29208, United States; orcid.org/0000-0003-4208-4815

Arjen Van Veelen – Stanford Synchrotron Radiation Lightsource, SLAC National Accelerator Laboratory, Menlo Park, California 94025, United States

John R. Bargar – Stanford Synchrotron Radiation Lightsource, SLAC National Accelerator Laboratory, Menlo Park, California 94025, United States; orcid.org/0000-0001-9303-4901

Theodore M. Besmann – Nuclear Engineering Program, University of South Carolina, Columbia, South Carolina 29208, United States

Kyle S. Brinkman – Department of Materials Science and Engineering, Clemson University, Clemson, South Carolina 29634-0901, United States; orcid.org/0000-0002-2219-1253

Complete contact information is available at:
<https://pubs.acs.org/10.1021/acs.jpcc.1c07552>

Author Contributions

[†]Co-first authors.

Notes

The authors declare no competing financial interest.

ACKNOWLEDGMENTS

The authors are grateful for the support of the Nuclear Energy University Program of the US Department of Energy Award ID: DE-NE0008772, 18-15065: “*in situ* Measurement and Validation of Uranium Molten Salt Properties at Operationally Relevant Temperatures”. Portions of this research were carried out at the Stanford Synchrotron Radiation Lightsource, a national user facility operated by Stanford University on behalf of the U.S. Department of Energy, Office of Basic Energy Sciences. The authors thank Piero Pianetta for his invaluable insight during the conceptual design of this experiment, Simon R. Bare and Adam S. Hoffman (SLAC) for assistance with X-ray absorption spectroscopy experimental design, measurement, data analysis, and careful reading of the manuscript, Ryan C. Davis (SLAC) for useful discussions on experimental design and for assistance with the X-ray absorption spectroscopy measurements, Alexey Boubnov (SLAC) for assistance with the X-ray absorption spectroscopy data collection, and Douglas Van Campen (SLAC) for assistance in setting up the heater at SSRL. The authors thank Amir M. Mofrad for discussions on evaluating the salt mixture melting points and Mina Aziziha for ICP-OES elemental composition analysis of the salt mixtures used in this study.

REFERENCES

- (1) Bessada, C.; Rakhmatullin, A.; Rollet, A. L.; Zanghi, D. High Temperature NMR Approach of Mixtures of Rare Earth and Alkali Fluorides: An Insight into the Local Structure. *J. Fluorine Chem.* **2009**, *130*, 45–52.
- (2) Williams, D. F.; Britt, P. F. *Technology and Applied R&D Needs for Molten Salt Chemistry*, Report for the US Department of Energy, Office of Nuclear Energy Molten Salt Chemistry Workshop, 2017.
- (3) Polovov, I. B.; Volkovich, V. A.; Charnock, J. M.; Kralj, B.; Lewin, R. G.; Kinoshita, H.; May, I.; Sharrad, C. A. In Situ Spectroscopy and Spectroelectrochemistry of Uranium in High-Temperature Alkali Chloride Molten Salts. *Inorg. Chem.* **2008**, *47*, 7474–7482.
- (4) Dent, A. J.; Welton, T.; Seddon, K. R.; Welton, T. The Structure of Halogenometallate Complexes Dissolved in Both Basic and Acidic Room-Temperature Halogenoaluminate(111) Ionic Liquids, as Determined by EXAFS. *J. Chem. Soc. Chem. Commun.* **1990**, 315–316.
- (5) Moon, J.; Abney, C.; Dolzhenkov, D.; Kurley, J. M.; Beyer, K. A.; Wright, J.; Dai, S.; Mayes, R. T.; Raiman, S. S. *Application of In Situ X-Ray Absorption Spectroscopy to Study Dilute Chromium Ions in a Molten Chloride Salt*; ChemRxiv, 2019. <https://doi.org/10.26434/chemrxiv.9959807.v1>.
- (6) Gill, S. K.; Huang, J.; Mausz, J.; Gakhar, R.; Roy, S.; Vila, F.; Topsakal, M.; Phillips, W. C.; Layne, B.; Mahurin, S.; Halstenberg, P.; Dai, S.; Wishart, J. F.; Bryantsev, V. S.; Frenkel, A. I. Connections between the Speciation and Solubility of Ni(II) and Co(II) in Molten ZnCl₂. *J. Phys. Chem. B* **2020**, *124*, 1253–1258.
- (7) Ishii, Y.; Sato, K.; Salanne, M.; Madden, P. A.; Ohtori, N. Thermal Conductivity of Molten Alkali Metal Fluorides (LiF, NaF, KF) and Their Mixtures. *J. Phys. Chem. B* **2014**, *118*, 3385–3391.
- (8) Gheribi, A. E.; Corradini, D.; Dewan, L.; Chartrand, P.; Simon, C.; Madden, P. A.; Salanne, M. Prediction of the Thermophysical Properties of Molten Salt Fast Reactor Fuel from First-Principles. *Mol. Phys.* **2014**, *112*, 1306–1312.
- (9) Dewan, L. C.; Simon, C.; Madden, P. A.; Hobbs, L. W.; Salanne, M. Molecular Dynamics Simulation of the Thermodynamic and Transport Properties of the Molten Salt Fast Reactor Fuel LiF-ThF₄. *J. Nucl. Mater.* **2013**, *434*, 322–327.
- (10) Capelli, E.; Beneš, O.; Konings, R. J. M. Thermodynamic Assessment of the LiF-ThF₄-PuF₃-UF₄ System. *J. Nucl. Mater.* **2015**, *462*, 43–53.
- (11) Pauvert, O.; Zanghi, D.; Salarme, M.; Simon, C.; Rakhmatullin, A.; Matsuura, H.; Okamoto, Y.; Vivet, F.; Bessada, C. In Situ Experimental Evidence for a Nonmonotonous Structural Evolution with Composition in the Molten LiF-ZrF₄ System. *J. Phys. Chem. B* **2010**, *114*, 6472–6479.
- (12) Matsuura, H.; Watanabe, S.; Akatsuka, H.; Okamoto, Y.; Adya, A. K. XAFS Analyses of Molten Metal Fluorides. *J. Fluorine Chem.* **2009**, *130*, 53–60.
- (13) Corradini, D.; Madden, P. A.; Salanne, M. Coordination Numbers and Physical Properties in Molten Salts and Their Mixtures. *Faraday Discuss.* **2016**, *190*, 471–486.
- (14) Hirata, S.; Gilliard, K.; He, X.; Li, J.; Sode, O. Ab Initio Molecular Crystal Structures, Spectra, and Phase Diagrams. *Acc. Chem. Res.* **2014**, *47*, 2721–2730.
- (15) Penner-Hahn, J. E. X-Ray Absorption Spectroscopy. In *Comprehensive Coordination Chemistry II*; Elsevier, 2003; Vol. 2, pp 159–186.
- (16) Crozier, E. D.; Alberding, N.; Sundheim, B. R. EXAFS Study of Bromomanganate Ions in Molten Salts. *J. Chem. Phys.* **1983**, *79*, 939–943.
- (17) Pauvert, O.; Salanne, M.; Zanghi, D.; Simon, C.; Reguer, S.; Thiaudière, D.; Okamoto, Y.; Matsuura, H.; Bessada, C. Ion Specific Effects on the Structure of Molten AF-ZrF₄ Systems (A+ = Li+, Na+, and K+). *J. Phys. Chem. B* **2011**, *115*, 9160–9167.
- (18) Dracopoulos, V.; Vagelatos, J.; Papatheodorou, G. N. Raman Spectroscopic Studies of Molten ZrF₄-KF Mixtures and of A₂ZrF₆, A₃ZrF₇ (A = Li, K or Cs) Compounds. *J. Chem. Soc., Dalton Trans.* **2001**, *7*, 1117–1122.

- (19) Lin, I.; Navrotsky, A.; Ballato, J.; Riman, R. E. High-Temperature Calorimetric Study of Glass-Forming Fluorozirconates. *J. Non-Cryst. Solids* **1997**, *215*, 113–124.
- (20) Fedorov, P. P. Glass Formation Criteria for Fluoride Systems. *Inorg. Mater.* **1997**, *33*, 1197–1205.
- (21) Novoselova, A. V.; Korenev, Y. M.; Simanov, Y. P. Research on the System LiF-ZrF₄. *Dokl. Akad. Nauk SSSR* **1961**, *139*, 892–894.
- (22) Ocadiz-Flores, J. A.; Capelli, E.; Raison, P. E.; Konings, R. J. M.; Smith, A. L. Thermodynamic Assessment of the LiF-NiF₂, NaF-NiF₂ and KF-NiF₂ Systems. *J. Chem. Thermodyn.* **2018**, *121*, 17–26.
- (23) Schreyer, D.; Waschk, V.; Chatelain, A. Raman Spectroscopy in Small Crystals of SrCl₂. *Surf. Sci.* **1981**, *106*, 336–344.
- (24) Smith, A. L.; Verleg, M. N.; Vlieland, J.; de Haas, D.; Ocadiz-Flores, J. A.; Martin, P.; Rothe, J.; Dardenne, K.; Salanne, M.; Gheribi, A. E.; Capelli, E.; van Eijck, L.; Konings, R. J. M. In Situ High-Temperature EXAFS Measurements on Radioactive and Air-Sensitive Molten Salt Materials. *J. Synchrotron Radiat.* **2019**, *26*, 124–136.
- (25) Rollet, A. L.; Bessada, C.; Auger, Y.; Melin, P.; Gailhanou, M.; Thiaudiere, D. A New Cell for High Temperature EXAFS Measurements in Molten Rare Earth Fluorides. *Nucl. Instrum. Methods Phys. Res., Sect. B* **2004**, *226*, 447–452.
- (26) Bessada, C.; Zanghi, D.; Pauvert, O.; Maksoud, L.; Gil-Martin, A.; Sarou-Kanian, V.; Melin, P.; Brassamin, S.; Nezu, A.; Matsuura, H. High Temperature EXAFS Experiments in Molten Actinide Fluorides: The Challenge of a Triple Containment Cell for Radioactive and Aggressive Liquids. *J. Nucl. Mater.* **2017**, *494*, 192–199.
- (27) Kiss, A. M.; Harris, W. M.; Nakajo, A.; Wang, S.; Vila-Comamala, J.; Deriy, A.; Chiu, W. K. S. In Situ Heater Design for Nanoscale Synchrotron-Based Full-Field Transmission X-Ray Microscopy. *Microsc. Microanal.* **2015**, *21*, 290–297.
- (28) Ravel, B.; Newville, M. ATHENA, ARTEMIS, HEPHAESTUS: Data Analysis for X-Ray Absorption Spectroscopy Using IFEFFIT. *J. Synchrotron Radiat.* **2005**, *12*, 537–541.
- (29) Stern, E. A. Number of Relevant Independent Points in X-Ray-Absorption Fine-Structure Spectra. *Phys. Rev. B* **1993**, *48*, 9825–9827.
- (30) Downward, L.; Booth, C. H.; Lukens, W. W.; Bridges, F. A Variation of the F-Test for Determining Statistical Relevance of Particular Parameters in EXAFS Fits. *AIP Conf. Proc.* **2007**, *882*, 129–131.
- (31) Rehr, J. J.; Kas, J. J.; Vila, F. D.; Prange, M. P.; Jorissen, K. Parameter-Free Calculations of X-Ray Spectra with FEFF9. *Phys. Chem. Chem. Phys.* **2010**, *12*, 5503–5513.
- (32) Bale, C. W.; Bélisle, E.; Chartrand, P.; Decterov, S. A.; Eriksson, G.; Gheribi, A. E.; Hack, K.; Jung, I.-H.; Kang, Y.-B.; Melançon, J.; Pelton, A. D.; Petersen, S.; Robelin, C.; Sangster, J.; Spencer, P.; Van Ende, M.-A. FactSage Thermochemical Software and Databases, 2010–2016. *Calphad* **2016**, *54*, 35–53.
- (33) Ard, J.; Johnson, K.; Christian, M.; Schorne Pinto, J.; Yingling, J.; Besmann, T. M.; McMurray, J. W.; Peng, J. FY20 Status Report on the Molten Salt Thermodynamic Database (MSTDB) Development. Oak Ridge National Laboratory, ORNL/SPR-2020/1648, September 2020.
- (34) Lide, D. R. *CRC Handbook of Chemistry and Physics*, 72nd ed.; CRC Press: Boca Raton, 1991.
- (35) Okamoto, Y.; Yaita, T.; Minato, K. High-Temperature XAFS Study of Solid and Molten SrCl₂. *J. Non-Cryst. Solids* **2004**, *333*, 182–186.
- (36) Walther, C.; Rothe, J.; Fuss, M.; Büchner, S.; Koltsov, S.; Bergmann, T. Investigation of Polynuclear Zr(IV) Hydroxide Complexes by Nanoelectrospray Mass-Spectrometry Combined with XAFS. *Anal. Bioanal. Chem.* **2007**, *388*, 409–431.
- (37) D'Angelo, P.; Migliorati, V.; Sessa, F.; Mancini, G.; Persson, I. XANES Reveals the Flexible Nature of Hydrated Strontium in Aqueous Solution. *J. Phys. Chem. B* **2016**, *120*, 4114–4124.
- (38) Mountjoy, G.; Pickup, D. M.; Anderson, R.; Wallidge, G. W.; Mark, A.; Newport, J.; Smith, M. E. Changes in the Zr Environment in Zirconia–Silica Xerogels with Composition and Heat Treatment as Revealed by Zr K-Edge XANES and EXAFS. *Phys. Chem. Chem. Phys.* **2000**, *2*, 2455–2460.
- (39) Sanchez, C.; In, M. Molecular Design of Alkoxide Precursors for the Synthesis of Hybrid Organic-Inorganic Gels. *J. Non-Cryst. Solids* **1992**, *147–148*, 1–12.
- (40) Bessada, C.; Rakhmatullin, A.; Rollet, A. L.; Zanghi, D. Lanthanide and Actinide Speciation in Molten Fluorides: A Structural Approach by NMR and EXAFS Spectroscopies. *J. Nucl. Mater.* **2007**, *360*, 43–48.
- (41) Grande, T.; Aasland, S.; Julsrud, S. A Differential Thermal Analysis Cell Suitable for Systems with Vapour Pressures Exceeding Ambient. *Thermochim. Acta* **1995**, *256*, 33–46.
- (42) Wyckoff, R. W. G. *Crystal Structures*, 2nd ed.; Interscience Publishers: New York, NY, 1963; Vol. 1.
- (43) Papiernik, R.; Mercurio, D.; Frit, B. Structure Du Tétrafluorure de Zirconium, ZrF₄[Alpha]. *Acta Crystallogr., Sect. B: Struct. Crystallogr. Cryst. Chem.* **1982**, *38*, 2347–2353.
- (44) Brunton, G. D.; Insley, H.; McVay, T. N.; Thoma, R. E. *Crystallographic Data for Some Metal Fluorides, Chlorides, and Oxides*, Report No. ORNL-3761; Oak Ridge National Laboratory: Oak Ridge, Tennessee, 1965.
- (45) Thoma, R. E.; Insley, H.; Friedman, H. A.; Hebert, G. M. Condensed System LiF-NaF-ZrF₄-Phase Equilibria and Crystallographic Data. *J. Chem. Eng. Data* **1965**, *10*, 219–230.
- (46) Dugat, P.; El-Ghozzi, M.; Metin, J.; Avignant, D. Crystal Structures of Li₄ZrF₈ and Li₃Zr₄F₁₉ and Reinvestigation of the LiF-ZrF₄ Phase Diagram. *J. Solid State Chem.* **1995**, *120*, 187–196.
- (47) Crystalline Structures of Several Zr Compounds by the National Science Center Kharkiv Institute of Physics and Technology.
- (48) Beneš, O.; Konings, R. J. M. Thermodynamic Study of LiF-BeF₂-ZrF₄-UF₄ System. *J. Alloys Compd.* **2008**, *452*, 110–115.
- (49) Sadoc, A.; Guillo, R. Spectres Raman de SrCl₂, BaCl₂ et PbCl₂. *C. R. Seances Acad. Sci., Ser. B* **1971**, *273*, 204–207.
- (50) Denham, P. A.; Marse, P. L. R.; Wilkinson, G. R. The Phonon Dispersion Curves, Infra-Red and Raman Spectra of SrCl₂. *J. Phys. C: Solid State Phys.* **1973**, *6*, No. 2066.
- (51) Shand, M.; Hanson, R. C.; Derrington, C. E.; O'Keeffe, M. An X-Ray and Raman Study of the Diffuse Transition in SrCl₂. *Solid State Commun.* **1976**, *18*, 769–772.
- (52) Mead, D. G.; Wilkinson, G. R. The Temperature Dependence of the Raman Spectra of Some Alkaline Earth Crystals with the Fluorite Structure. *J. Phys. C: Solid State Phys.* **1977**, *10*, No. 1063.
- (53) Papatheodorou, G. N.; Yannopoulos, S. N. Light Scattering from Molten Salts: Structure and Dynamics. In *Molten Salts: From Fundamentals to Applications*; Gaune-Escard, M., Ed.; Springer: Dordrecht, 2011; pp 47–106.
- (54) Drago, R. S. *Physical Methods for Chemists*, 2nd ed.; Saunders College Publishing, 1992.
- (55) Kawamoto, Y.; Sakaguchi, F. Thermal Properties and Raman Spectra of Crystalline and Vitreous BaZrF₆, Pb ZrF₆, and SrZrF₆. *Bull. Chem. Soc. Jpn.* **1983**, *56*, 2138–2141.
- (56) Toth, L. M.; Quist, A. S.; Boyd, G. E. Raman Spectra of Zirconium(IV) Fluoride Complex Ions in Fluoride Melts and Polycrystalline Solids. *J. Phys. Chem. A* **1973**, *77*, 1384–1388.
- (57) Phifer, C. C.; Goztoła, D. J.; Kieffer, J.; Angell, C. A. Effects of Coordination Environment on the Zr–F Symmetric Stretching Frequency of Fluorozirconate Glasses, Crystals, and Melts. *J. Chem. Phys.* **1991**, *94*, 3440–3450.
- (58) Aasland, S.; Einarsrud, M. A.; Grande, T.; McMillan, P. F. Spectroscopic Investigations of Fluorozirconate Glasses in the Ternary Systems ZrF₄-BaF₂-AF (A = Na, Li). *J. Phys. Chem. B* **1996**, *100*, 5457–5463.
- (59) Badger, R. M. The Relation Between the Internuclear Distances and Force Constants of Molecules and Its Application to Polyatomic Molecules. *J. Chem. Phys.* **1935**, *3*, 710–714.
- (60) Inoue, S.; Nishizawa, M.; Kawazoe, H.; Yamane, M. Raman Spectra of the Melt of ZrF₄-BaF₂-LaF₃-AlF₃-NaF (or LiF) Systems. *Mater. Sci. Forum* **1988**, *32–33*, 447–452.
- (61) Coupe, R.; Louer, D.; Lucas, J.; Leonard, A. J. X-Ray Scattering Studies of Glasses in the System ZrF₄-BaF₂. *J. Am. Ceram. Soc.* **1983**, *66*, 523–529.

(62) Boulard, B.; Le Bail, A.; Laval, J. P.; Jacoboni, C. Local Environment of Zr in Barium Fluorozirconate Glasses: The EXAFS Point of View. *J. Phys. Colloques* **1986**, *47*, 791–794.

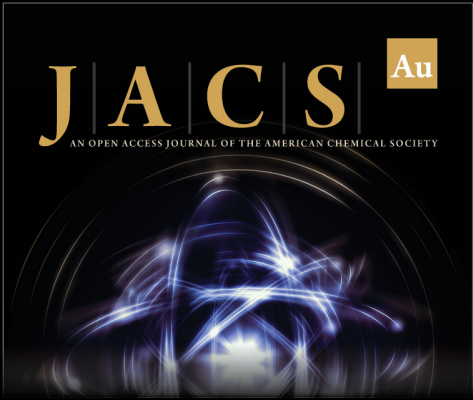
(63) Badger, R. M. A Relation Between Internuclear Distances and Bond Force Constants. *J. Chem. Phys.* **1934**, *2*, 128–131.

(64) Dracopoulos, V.; Vagelatos, J.; Papatheodorou, G. N. Raman Spectroscopic Studies of Molten ZrF₄–KF Mixtures and of A₂ZrF₆, A₃ZrF₇ (A = Li, K or Cs) Compounds. *J. Chem. Soc., Dalton Trans.* **2001**, *7*, 1117–1122.


(65) Raptis, C. Determination of Absolute Light-Scattering Cross Sections of Molten Salts. *J. Appl. Phys.* **1986**, *59*, 1644–1652.


(66) Welsh, H. L.; Crawford, M. F.; Staple, W. J. Raman Spectrum of Rocksalt. *Nature* **1949**, *164*, 737–738.


(67) Möller, W.; Kaiser, R. Impurity-Induced and Second Order Raman Spectra of NaCl Crystals Doped with Different Ag⁺ Concentrations. *Z. Naturforsch., A* **1970**, *25*, 1024–1029.



JACS Au
AN OPEN ACCESS JOURNAL OF THE AMERICAN CHEMICAL SOCIETY

 Editor-in-Chief
Prof. Christopher W. Jones
Georgia Institute of Technology, USA

Open for Submissions 

pubs.acs.org/jacsau  ACS Publications
Most Trusted. Most Cited. Most Read.

Supporting Information

In situ Determination of Speciation and Local Structure of NaCl-SrCl₂ and LiF-ZrF₄ Molten Salts

Timothy J. Lynch^{*,1}, Nancy R. Birkner^{*,2}, Matthew S. Christian³, Jacob A. Wrubel¹, Juliano Schorne-Pinto³, Arjen Van Veelen⁴, John R. Bargar⁴, Theodore M. Besmann³, Kyle S. Brinkman² and Wilson K. S. Chiu^{#,1}

¹ Department of Mechanical Engineering, University of Connecticut, Storrs, CT 06369-3139, USA.

² Department of Materials Science and Engineering, Clemson University, Clemson, SC 29634-0901, USA.

³ Nuclear Engineering Program, University of South Carolina, Columbia, SC 29208, USA.

⁴ Stanford Synchrotron Radiation Lightsource, SLAC National Accelerator Laboratory, Menlo Park, CA 94025, USA.

* Co-first authors

Corresponding author (wchiu@engr.uconn.edu)

List of Tables

Table S1. Calculated EXAFS parameters for the 5 mol% SrCl₂:NaCl salt mixture.

Table S2. Calculated EXAFS parameters for the 5 mol% ZrF₄:LiF salt mixture.

Table S3. K-range and R-range window used for Fourier transforms to R-space for the 5 mol% SrCl₂ in NaCl salt mixture.

Table S4. K-ranges and R-range window used for Fourier transforms to R-space for the 5 mol% ZrF₄ in LiF salt mixture.

Table of Figures

Figure S1. (left) General form of the temperature programs used during DSC measurements under continuous Ar flow. (middle) Heat profile schema applied to the samples under continuous Ar flow, to ensure adventitious oxygen and water were not present in the samples prior to their measurement with DCS and Raman. (right) Linkam TS1500 high-temperature stage in which samples may be viewed through the Raman microscope for focusing the laser as well as to observe melting/fusion of samples.

Figure S2. (left) Experimental setup at the Stanford Synchrotron Radiation Lightsource, Beamline 11-2 for *in situ* x-ray absorption spectroscopy measurements. (right) Schematic of the sample holder and heater configurations.

Figure S3. R-space fits of SrCl₂-NaCl salt mixture from 25 °C to 1,000 °C recorded across the Sr K-edge. K-ranges used for the FT and fitting are shown in Table S3.

Figure S4. Comparison of FEFF calculated Li₂ZrF₆, Li₃Zr₄F₁₉, and Li₄ZrF₈ ternary formation to the 1,000 °C ZrF₄-LiF salt mixture recorded across the Zr K-edge.

Figure S5: Comparison of the resolidified 5% ZrF₄ in LiF molten salt mixture to FEFF calculated Li₄ZrF₈ in R- and K-space recorded across the Zr K-edge. The k-range for the Fourier transform is 3 Å⁻¹ to 9 Å⁻¹.

Figure S6. R-space fits of ZrF₄-LiF salt mixture from 25 °C to 1,100 °C recorded across the Zr K-edge. K-ranges used for FT and fitting are shown in Table S4.

Figure S7. K-space fits of the 5 mol% SrCl₂:NaCl salt mixture from 25 °C to 1,000 °C recorded across the Sr K-edge.

Figure S8. Im[R] fits of the 5 mol% SrCl₂:NaCl salt mixture from 25 °C to 1,000 °C recorded across the Sr K-edge. K-ranges used for Fourier transform and fitting are shown in Table S3.

Figure S9. K-space fits of the 5 mol% ZrF₄:LiF salt mixture from 25 °C to 1,100 °C recorded across the Zr K-edge.

Figure S10. Im[R] fits of the 5 mol% ZrF₄:LiF salt mixture from 25 °C to 1,100 °C recorded across the Zr K-edge. K-ranges used for Fourier transform and fitting are shown in Table S4.

Figure S11. Comparison of 2:1 ratio of (2:1) BN-diluted 5 mol% ZrF₄ in LiF fluoride salts with non-diluted at 600 °C: a) XANES comparison, b) k-space comparison c) R-space comparison with FT taken over the k-range 3 to 12. Measurements were performed across the Zr K-edge.

Tables

Table S1. Calculated EXAFS parameters for the 5 mol% SrCl₂:NaCl salt mixture.

	S_0^2	E_0	R (Å) Sr ²⁺ -Cl ⁻	σ^2 (Å ²)	N	3 rd Cumulant (Å)
25 °C	0.74	0.45(1.28)	3.01(0.01)	0.015(0.003)	7.5(1.3)	-
400 °C	0.74	-1.07(1.53)	2.94(0.08)	0.027(0.005)	6.5(1.4)	-
600 °C	0.74	-1.90(2.11)	2.92(0.10)	0.025(0.006)	6.5(1.9)	-
800 °C	0.74	1.37(2.52)	2.93(0.10)	0.019(0.003)	5.9(0.89)	0.003(0.002)
1,000 °C	0.74	3.05(2.88)	3.03(0.01)	0.026(0.004)	5.8(1.1)	0.008(0.003)

Table S2. Calculated EXAFS parameters for the 5 mol% ZrF₄:LiF salt mixture.

	S_0^2	E_0	R_1 (Å) Zr ⁴⁺ -F ⁻	R_2 (Å) Zr ⁴⁺ -F ⁻	σ^2 (Å ²)	N_1 (for R_1)	N_2 (for R_2)	N ($N_1 + N_2$)
25 °C	0.89	-2.81(1.54)	2.07(0.02)	2.21(0.02)	0.002(0.002)	4.7(0.91)	3.3(0.39)	8.0(0.99)
200 °C	0.89	-3.29(1.63)	2.07(0.01)	2.23(0.04)	0.002(0.002)	4.9(1.0)	3.1(0.35)	8.0(1.1)
400 °C	0.89	-3.22(1.52)	2.07(0.02)	2.23(0.04)	0.002(0.002)	4.7(0.96)	2.8(0.31)	7.5(1.0)
600 °C	0.89	-7.50(2.53)	2.05(0.04)	-	0.007(0.002)	6.2(1.1)	-	6.2(1.1)
700 °C	0.89	-5.67(3.04)	2.08(0.005)	-	0.009(0.003)	5.8(1.3)	-	5.75(1.3)
800 °C	0.89	-0.93(4.61)	2.13(0.04)	-	0.009(0.006)	3.9(1.6)	-	3.9(1.6)
1,000 °C	0.89	-2.73(6.13)	2.12(0.04)	-	0.012(0.008)	4.5(2.5)	-	4.5(2.5)
1,100 °C	0.89	5.09(2.44)	2.14(0.06)	-	0.013(0.004)	4.8(1.2)	-	4.8(1.2)

Table S3. K-range and R-range window used for Fourier transforms to R-space for the 5 mol% SrCl₂ in NaCl salt mixture.

Temperature	k-range	R-range window
25°C	3.1 Å ⁻¹ to 8.5 Å ⁻¹	1.35 Å to 3.5 Å
400°C	3 Å ⁻¹ to 7 Å ⁻¹	1.25 Å to 3.5 Å
600°C	3 Å ⁻¹ to 7.5 Å ⁻¹	1.45 Å to 3.5 Å
800°C	3 Å ⁻¹ to 7 Å ⁻¹	1.45 Å to 5 Å
1000°C	3 Å ⁻¹ to 6.6 Å ⁻¹	1.40 Å to 4.5 Å

Table S4. K-ranges and R-range window used for Fourier transforms to R-space for the 5 mol% ZrF₄ in LiF salt mixture.

Temperature	k-range	R-range window
25°C	3 Å ⁻¹ to 12 Å ⁻¹	1.15 Å to 3 Å
200°C	3 Å ⁻¹ to 11 Å ⁻¹	1.25 Å to 3 Å
400°C	3 Å ⁻¹ to 11 Å ⁻¹	1.25 Å to 3.5 Å
600°C	3 Å ⁻¹ to 12 Å ⁻¹	1.15 Å to 2.4 Å
700°C	3 Å ⁻¹ to 11 Å ⁻¹	1.15 Å to 2.4 Å
800°C	3 Å ⁻¹ to 9 Å ⁻¹	1.15 Å to 2.5 Å
1000°C	3 Å ⁻¹ to 9 Å ⁻¹	1.35 Å to 2.6 Å
1100°C	3 Å ⁻¹ to 7.4 Å ⁻¹	1.45 Å to 5 Å

Figures

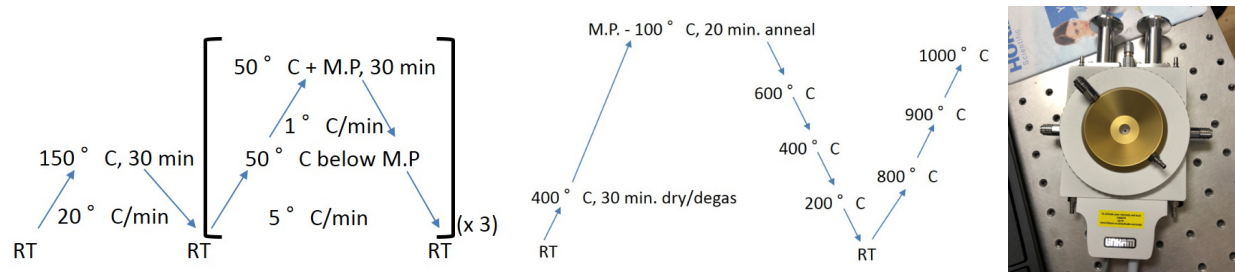


Figure S1: (left) General form of the temperature programs used during DSC measurements under continuous Ar flow. (middle) Heat profile schema applied to the samples under continuous Ar flow, to ensure adventitious oxygen and water were not present in the samples prior to their measurement with DCS and Raman. (right) Linkam TS1500 high-temperature stage in which samples may be viewed through the Raman microscope for focusing the laser as well as to observe melting/fusion of samples.

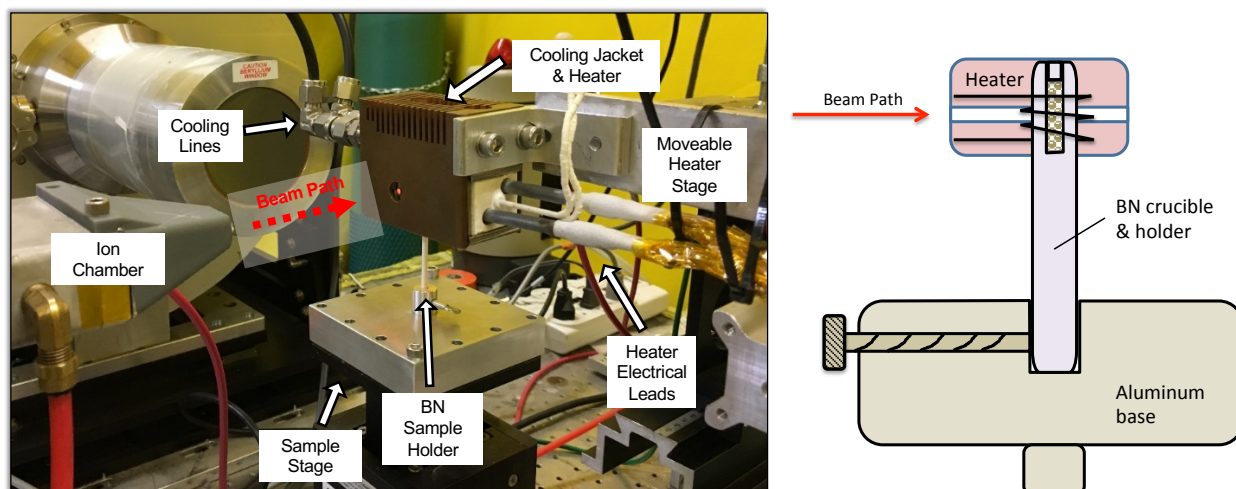


Figure S2. (left) Experimental setup at the Stanford Synchrotron Radiation Lightsource, Beamline 11-2 for *in situ* x-ray absorption spectroscopy measurements. (right) Schematic of the sample holder and heater configurations.

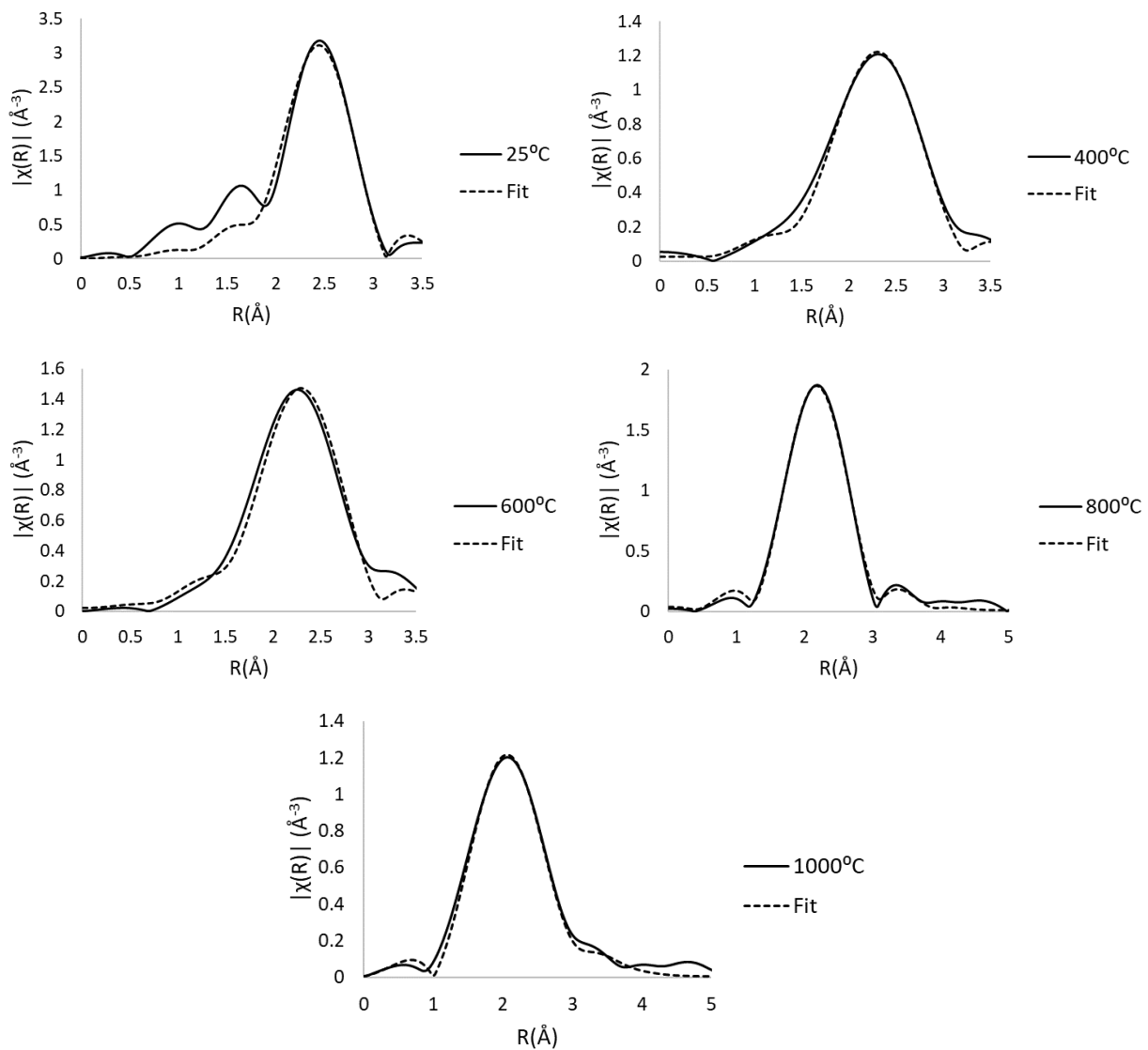


Figure S3. R-space fits of SrCl_2 - NaCl salt mixture from 25 °C to 1,000 °C recorded across the Sr K-edge. K-ranges used for the FT and fitting are shown in Table S3.

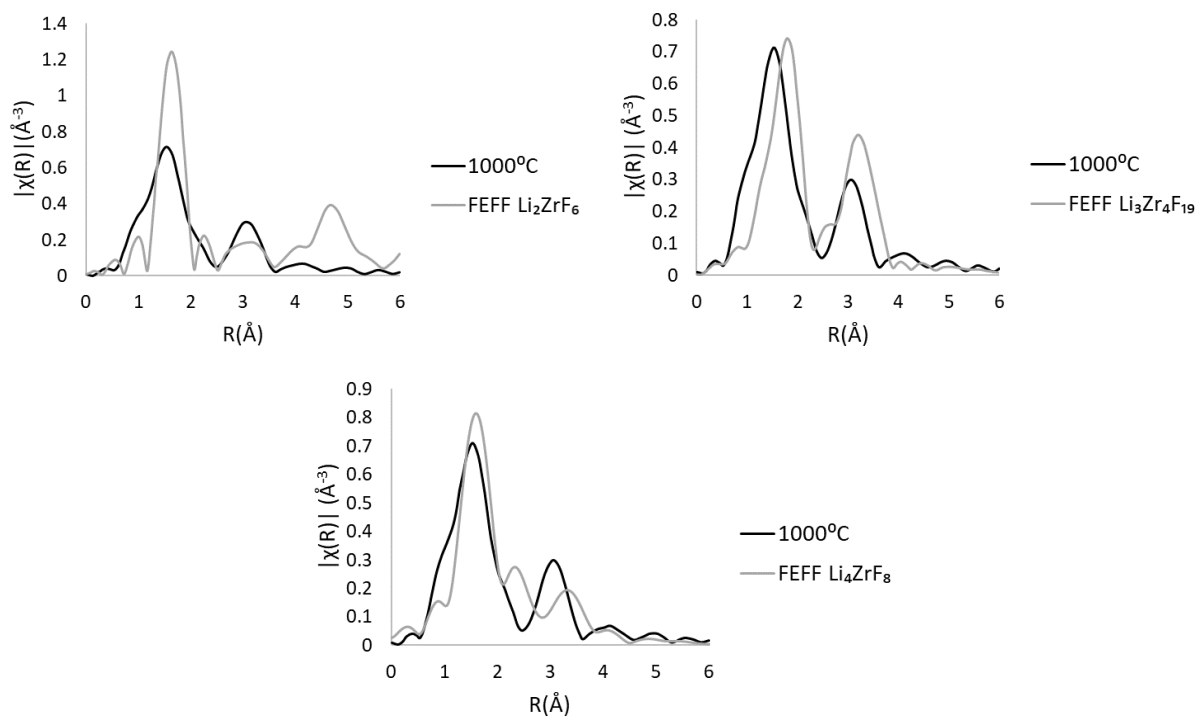


Figure S4. Comparison of FEFF calculated Li_2ZrF_6 , $\text{Li}_3\text{Zr}_4\text{F}_{19}$, and Li_4ZrF_8 ternary formation to the 1,000 °C ZrF_4 - LiF salt mixture recorded across the Zr K-edge.

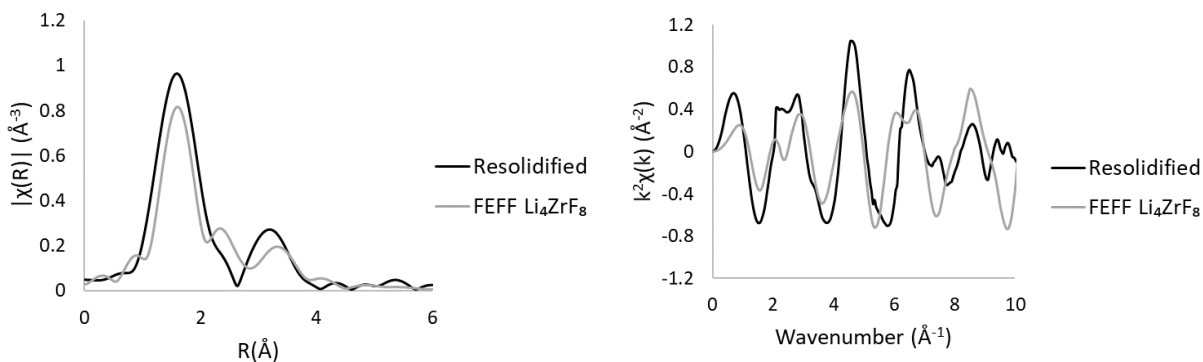


Figure S5: Comparison of the resolidified 5% ZrF_4 in LiF molten salt mixture to FEFF calculated Li_4ZrF_8 in R- and K-space recorded across the Zr K-edge. The k-range for the Fourier transform is 3 \AA^{-1} to 9 \AA^{-1} .

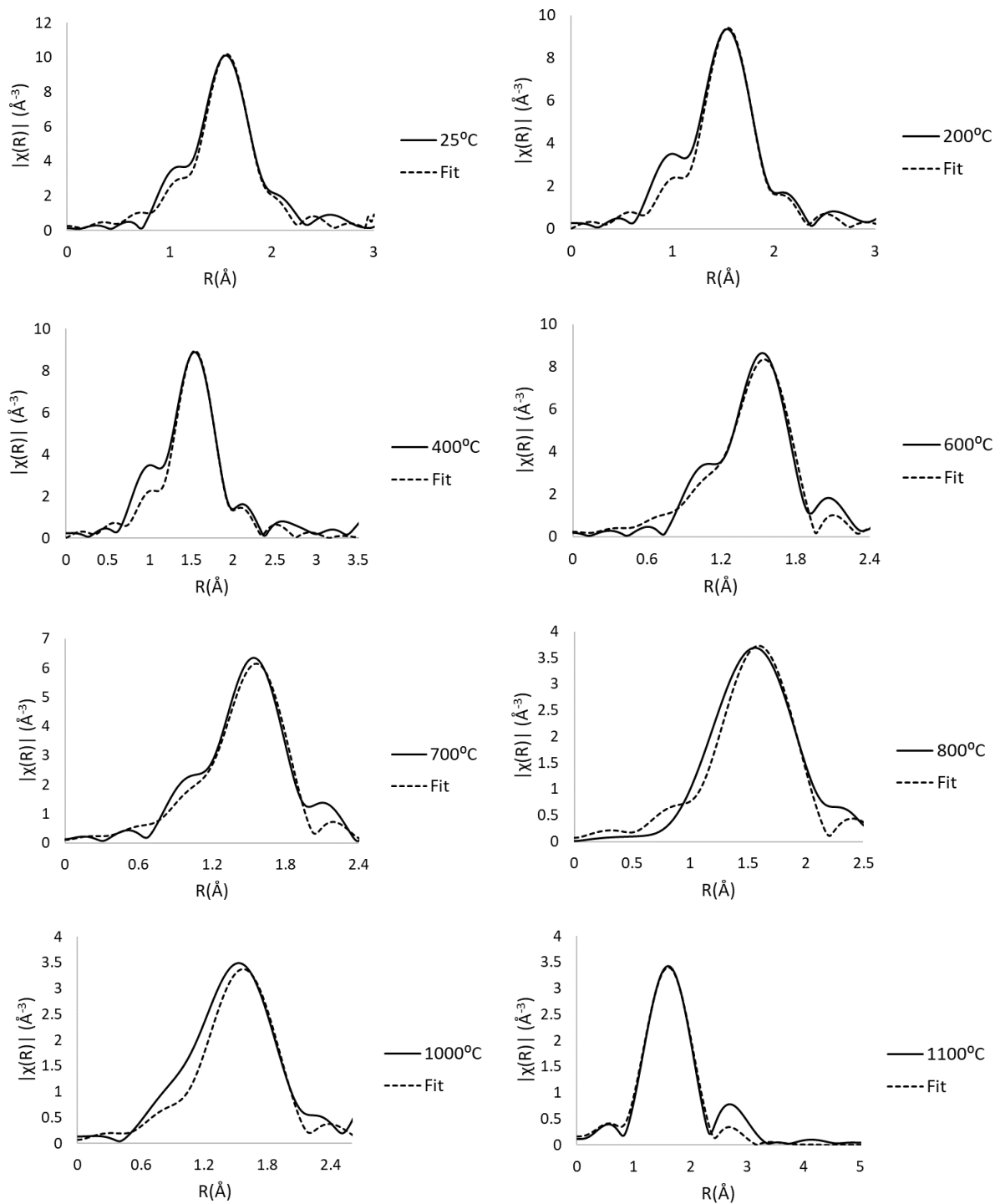


Figure S6. R-space fits of $\text{ZrF}_4\text{-LiF}$ salt mixture from 25 °C to 1,100 °C recorded across the Zr K-edge. K-ranges used for FT and fitting are shown in Table S4.

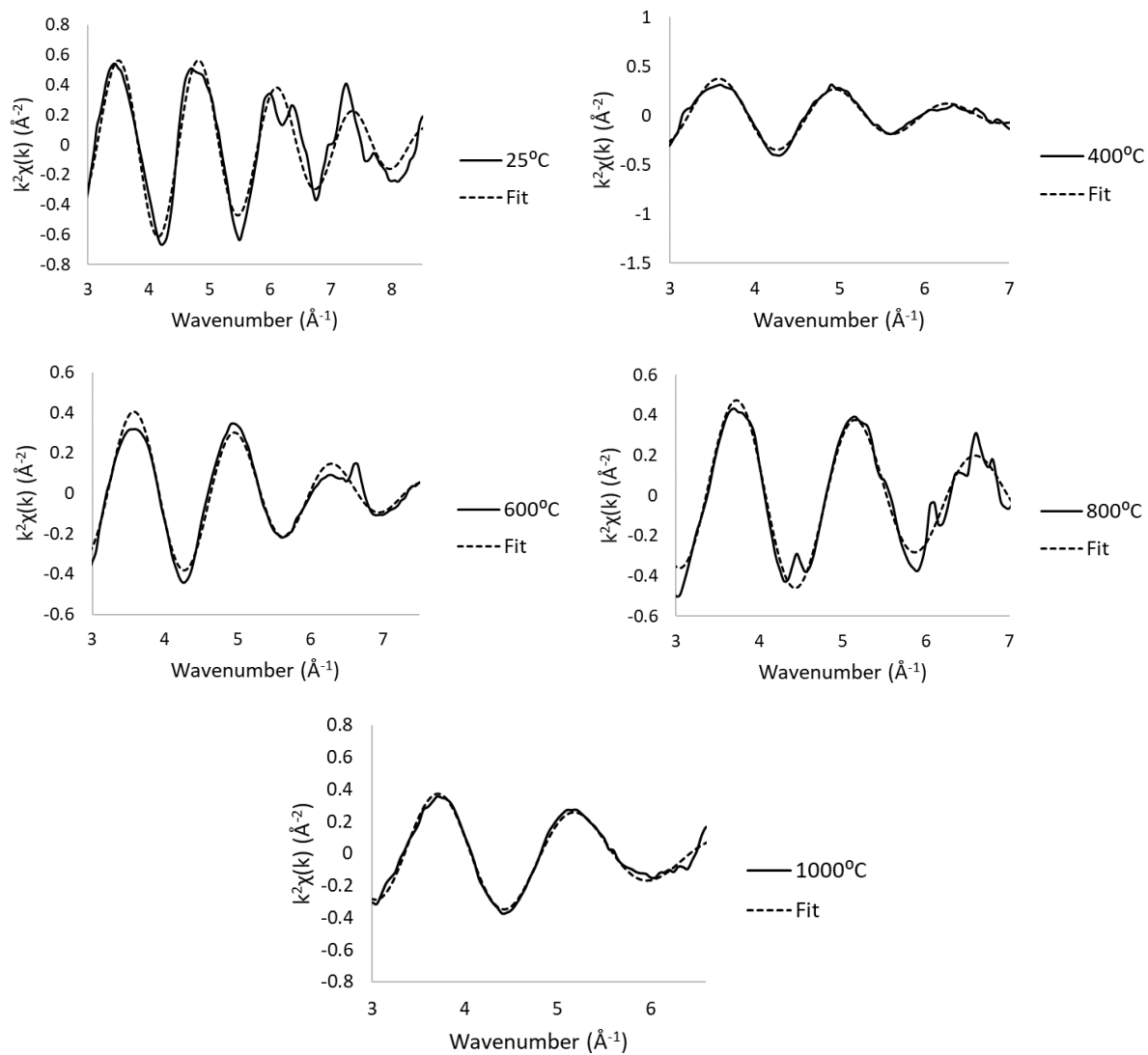


Figure S7. K-space fits of the 5 mol% SrCl₂:NaCl salt mixture from 25 °C to 1,000 °C recorded across the Sr K-edge.

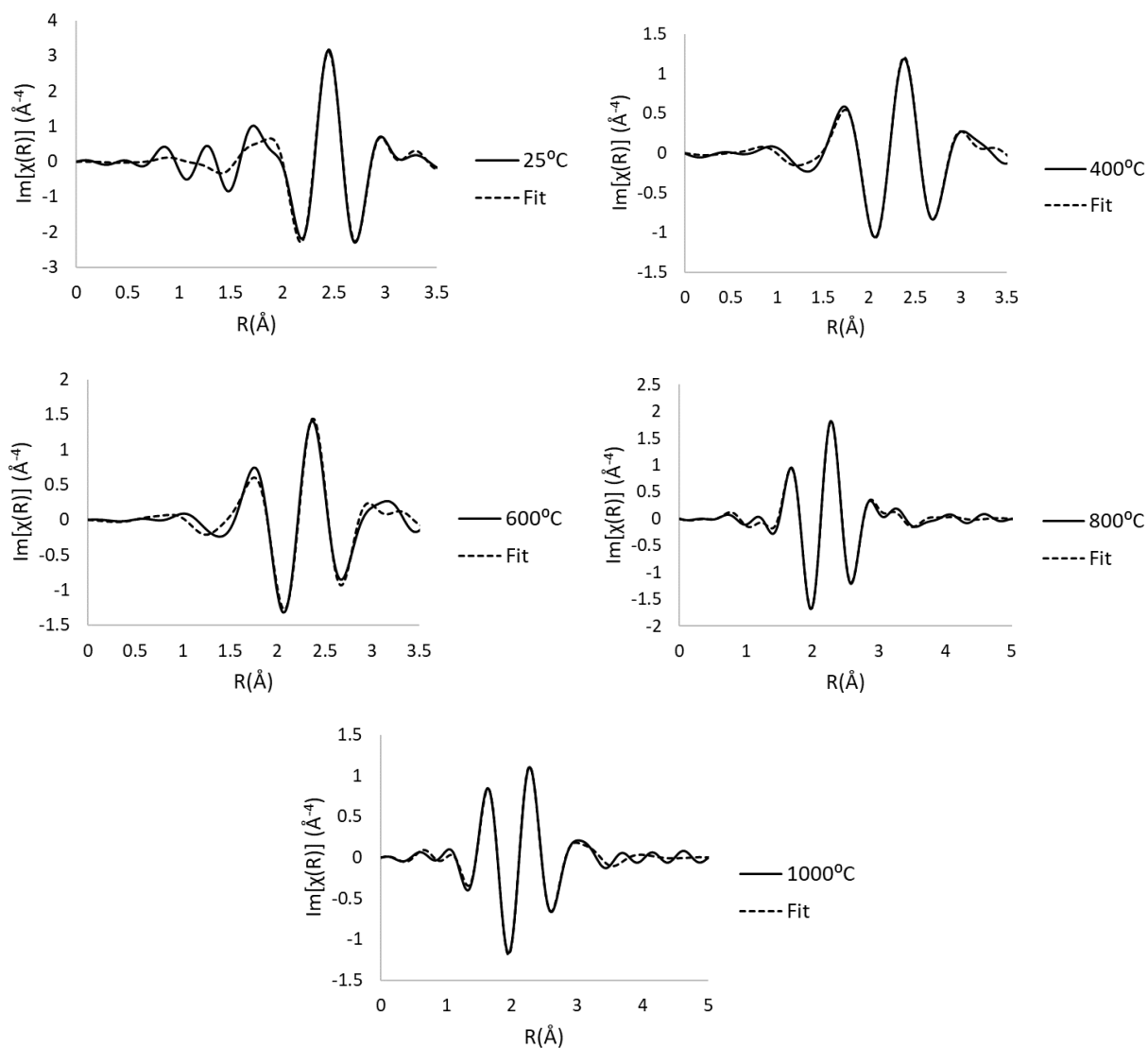


Figure S8. $\text{Im}[\chi(R)]$ fits of the 5 mol% $\text{SrCl}_2:\text{NaCl}$ salt mixture from 25 °C to 1,000 °C recorded across the Sr K-edge. K-ranges used for Fourier transform and fitting are shown in Table S3.

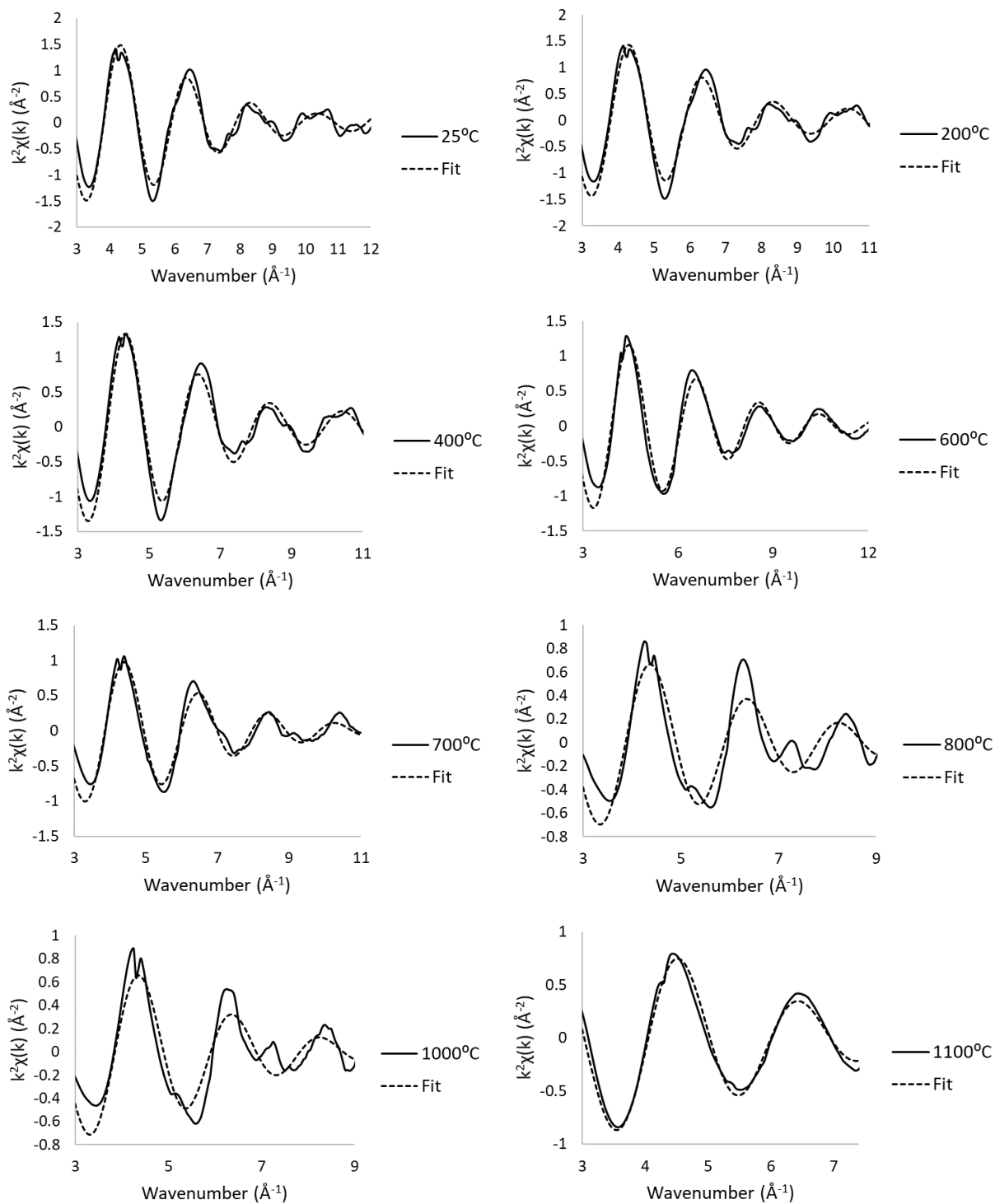


Figure S9. K-space fits of the 5 mol% ZrF₄:LiF salt mixture from 25 °C to 1,100 °C recorded across the Zr K-edge.

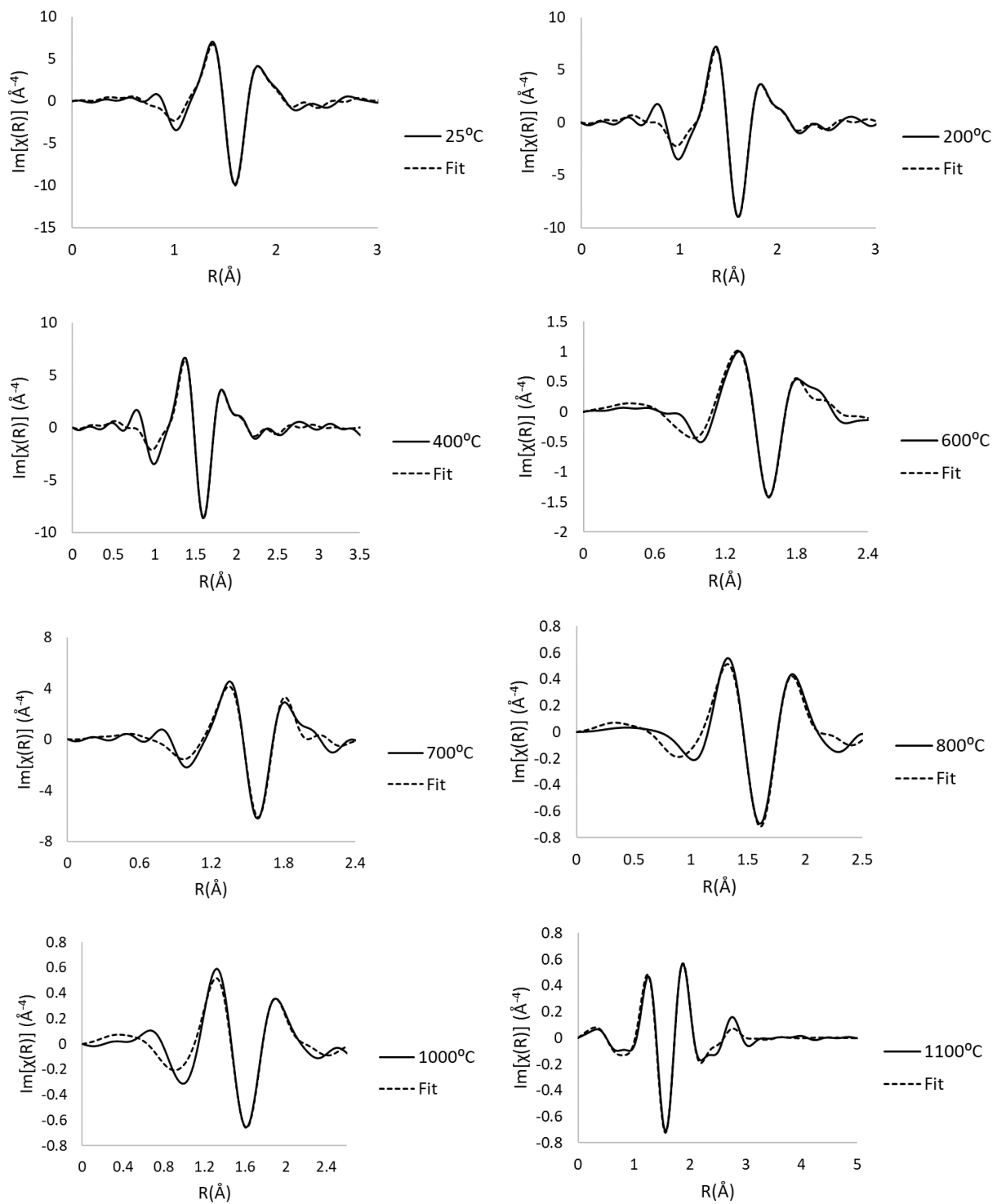


Figure S10. $\text{Im}[R]$ fits of the 5 mol% $\text{ZrF}_4:\text{LiF}$ salt mixture from 25 °C to 1,100 °C recorded across the Zr K-edge. K-ranges used for Fourier transform and fitting are shown in Table S4.

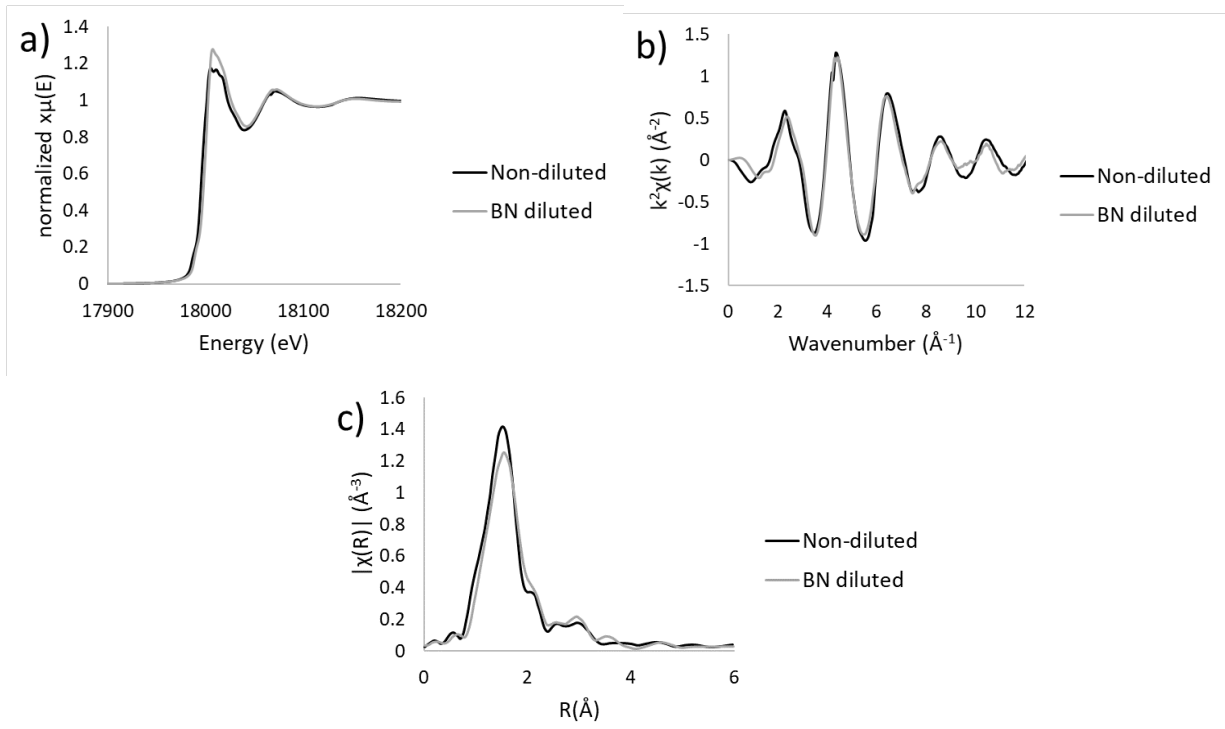


Figure S11. Comparison of 2:1 ratio of (2:1) BN-diluted 5 mol% ZrF_4 in LiF fluoride salts with non-diluted at 600 °C: a) XANES comparison, b) k-space comparison c) R-space comparison with FT taken over the k-range 3 to 12. Measurements were performed across the Zr K-edge.